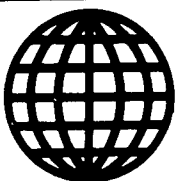


JPRS-JST-89-004

7 FEBRUARY 1989



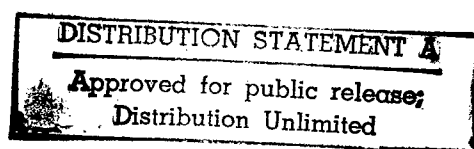
**FOREIGN
BROADCAST
INFORMATION
SERVICE**

JPRS Report

Science & Technology

Japan

FUNCTIONALLY GRADIENT MATERIALS SYMPOSIUM



19980701 051

JPRS-JST-89-004

7 FEBRUARY 1989

SCIENCE & TECHNOLOGY

JAPAN

FUNCTIONALLY GRADIENT MATERIALS SYMPOSIUM

43067606 Tokyo KEISHA KINO ZAIRYO KENKYUKAI in Japanese 1 Jul 88 pp 1-50

[Papers from the Second Symposium for Functionally Gradient Materials held 1 July 1988 in Tokyo, sponsored by the Functionally Gradient Materials Research Society.]

CONTENTS

Practical Aspects of Metal-Ceramic Joining Bound to Ceramic Machining.....	1
Functionally Gradient Materials in Designing Shuttle Engines.....	4
Problems With Exposed-to-Plasma Devices.....	7
Thermoelasticity Estimation Model for Polyphase Mixed Systems.....	13
Functionally Gradient Material Design Aid System.....	21
Functionally Gradient It-TiN, Cr-CrN Composites.....	27
Green Sheet Manufacture From Ceramics-Metal Powder.....	35
Metal-Ceramics Film Formation by Separate Thermal Spray.....	43
TiB ₂ -Cu FGM Synthesis by Self-Exothermic Reaction Method.....	48
Research on Si ₃ N ₄ -MO Ceramic With Gradient Composition.....	54
Research on FGM Thermal Property Evaluation Technique.....	62
Research on FGM Fracture Strength Evaluation.....	69

Practical Aspects of Metal-Ceramic Joining Bound to Ceramic Machining

43067606a Tokyo KEISHA KINO ZAIRYO KENKYUKAI in Japanese 1 Jul 88 pp 1-3

[Article by Michel Courbiere and Makoto Kinoshita: "Practical Aspects of Metal-Ceramic Joining Bound to Ceramic Machining, Compounds, and Interface Shapes"--in English]

[Text] In the extension use of ceramics, joining takes an important place in the ceramic industry. Several problems like difference between coefficients of thermal expansion or bad wetting of ceramics by molten metal must be solved. Joining conditions such [as] joining temperature, [and] furnace atmosphere are often as crucial but other parameters must be taken into account to improve high strength and good reliability.

In solid state bonding the most important factor which reduces these properties is the edge effect. In this area some voids can be formed during the compression and these zones can be the starting point of cracks. Several mechanisms promote the bonding between the metal and the ceramic: plastic deformation, creeping, diffusion, evaporation, condensation; besides those, interface macrostructure and ceramic roughness take an important place in the joining mechanical behavior. Figure 1 shows that mechanical anchorage due to the cavities on the ceramic enhances the bonding strength but also damages can be induced by grinding and affect hugely the joining.

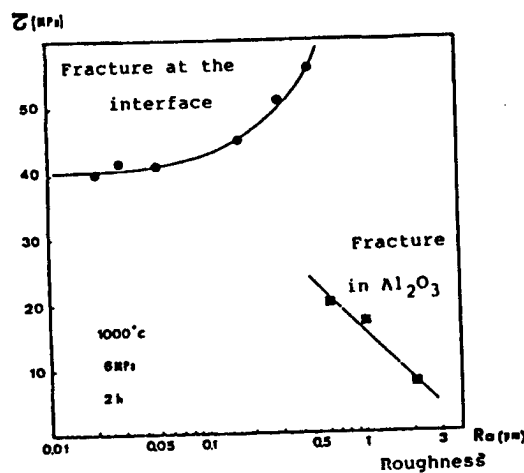


Figure 1.

Si_3N_4 /steel (Figure 2) joining does not present such phenomena because bonding strength is higher than that of Si_3N_4 and fracture occurs in the ceramic part in every case. In the case of Si_3N_4 /Ni (Figure 3), the same behavior observed with Al_2O_3 /Cu occurs but the higher toughness of Si_3N_4 prevents the grinding damage but the presence of new compounds limits the joining strength.

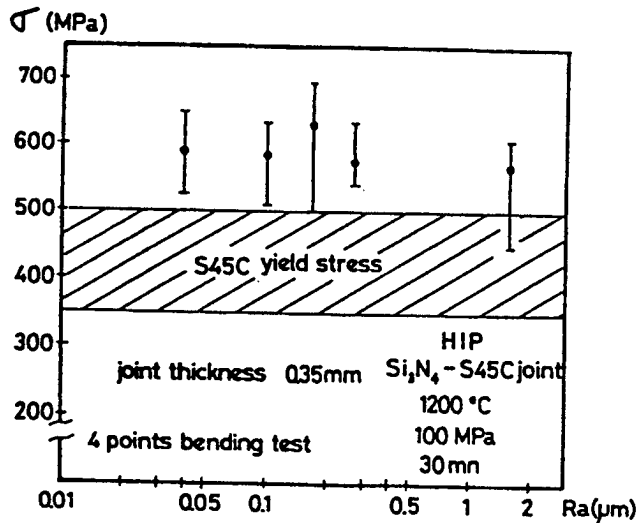


Figure 2.

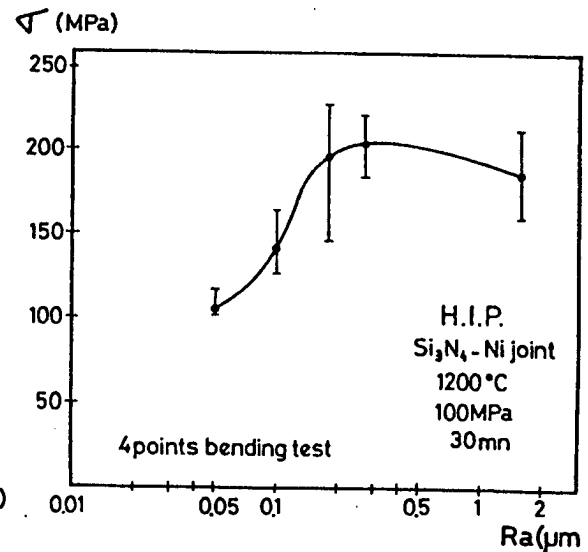


Figure 3.

In the case of brazing the structure of the brase alloys after cooling is also important. Recently the active brazing alloys used in Si_3N_4 joining can present some brittle properties which can lower the interface resistance even [when] good bonding with the ceramic is obtained. In the "gas eutectic method" employed in Al_2O_3 /Cu joining, the amount of oxygen in the brazing alloys, brought by copper oxidation at the interface, is an essential parameter. The lack of this element leads to a partial wetting of the ceramic, an excess creates residual Cu_2O ; both can hugely affect the strength (Figure 4). In this technique the weak point is not the presence of compounds at the interface but really the brazing structure.

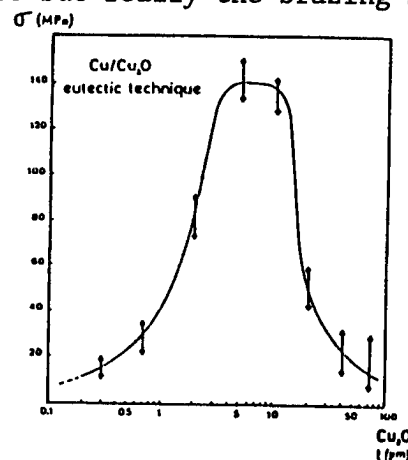


Figure 4.

Anyway it must be kept in mind that the principal factors, valid for all techniques, are the shape and the size of the joined parts; the best technique employed with small samples can be a failing if it is applied for large parts. Also extension to industrial use must be done taking some attention on these points.

Functionally Gradient Materials in Designing Shuttle Engines

43067606b Tokyo KEISHA KINO ZAIRYO KENKYUKAI in Japanese 1 Jul 88 pp 5-6

[Article by Kuniyasu Yamanaka, Ishikawajima-Harima Heavy Industries: "Functionally Gradient Materials Viewed From Standpoint of Designing Space Shuttle Engines"]

[Text] Space shuttles or spacecraft are manned vehicles capable of horizontal takeoff and landing. They are designed for repeated use for transporting materials between space and earth in support of man's future space activities. The requirements for them include low building cost, big payload, and a high level of safety.

Development of a space shuttle requires the solution of many technical problems. Among these, the development of a propulsion system that enables the space shuttle to reach a higher altitude at a wider range of speed than achieved so far assumes particular importance. It is estimated that a space shuttle traveling at superhigh speed will cause the maximum temperature of the environment in which the engine operates to exceed 3300 K.

Therefore, to realize a space shuttle propulsion system, it is essential to develop new high-heat-resistant materials. The materials drawing attention in this regard include FRCs [fiber reinforced composites], C/C [carbon fiber reinforced carbon composites], and functionally gradient materials.

In this article, the environmental and material requirements for the air turbo ram (ATR)--an engine being considered for use in space shuttles--will be reviewed, and the application of functionally gradient materials to the ATR will be discussed.

The temperatures that the main parts (the intake, fan, and compressor, turbine, combustor, and exhaust nozzle) of the ATR are expected to reach during flight at Mach 2 are indicated in Figure 1.

Figure 2 shows the specific strength-temperature characteristics of various materials; the specific strength is among the mechanical material properties to be considered in designing engine parts. The design specific strengths required for the main parts of the ATR are also indicated in Figure 2, for comparison with the corresponding values of existing materials. The target heat resistance of functionally gradient materials has been set at 2,000 K,

and they are being considered for use in the fan, turbine, and intake. In this connection, the design specific strength required is indicated as $(10-20) \times 10^6 \text{ mm}$.

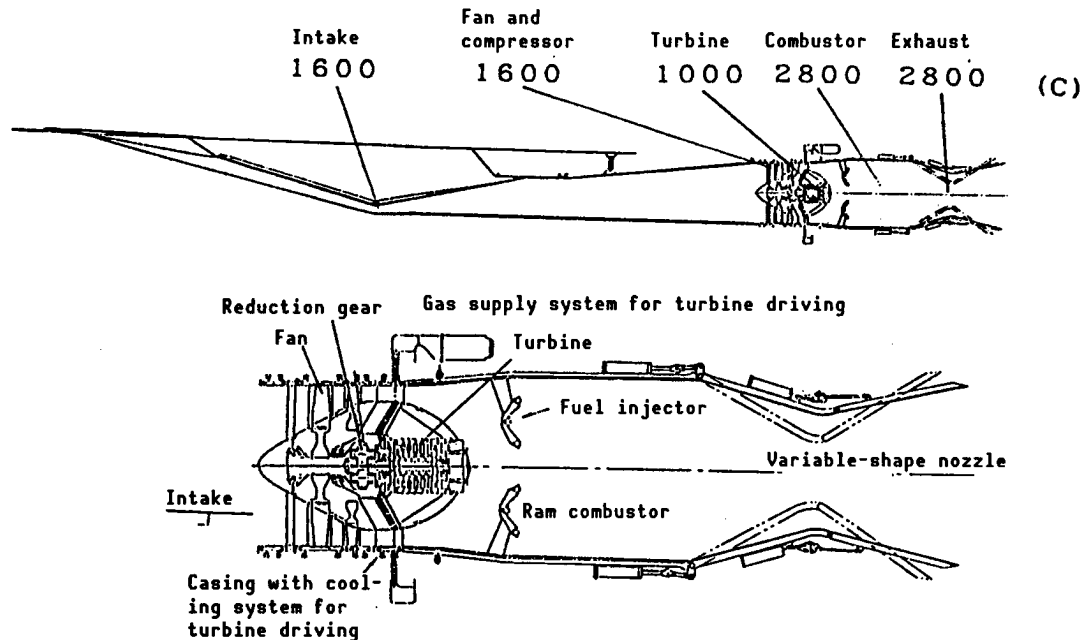


Figure 1. Operating Environment Temperatures for ATR (at Mach 6)

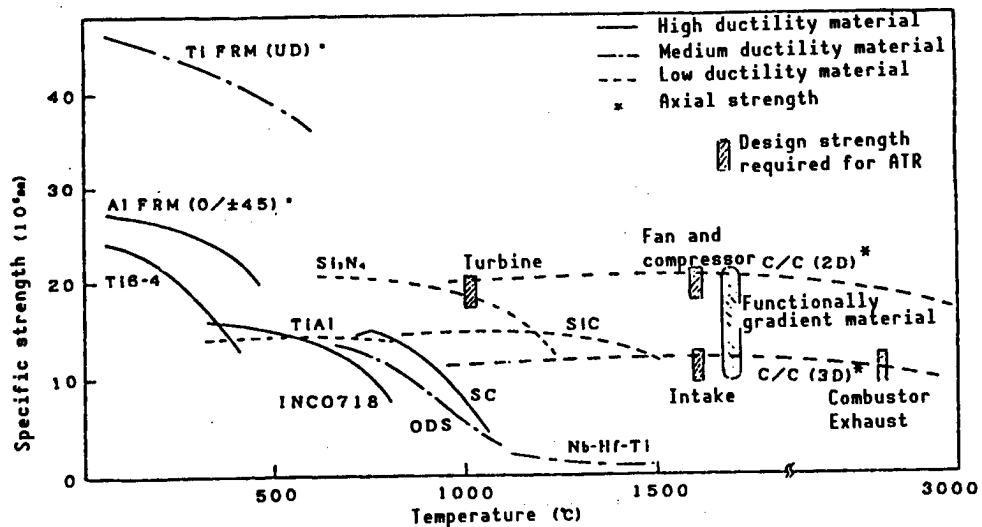


Figure 2. Required Material Strengths vs. Actual Material Strengths

The mechanical characteristics required of engine parts are dependent on whether they are rotary parts. In addition, individual parts must satisfy the respective specific requirements. Take the blades and disk in the fan and compressor section of the ATR, for example. They must have high static

strength and rigidity. In addition, it is also very important for them to be highly resistant to low-frequency fatigue and to possess high fracture toughness so that they can be used in repeated flights, i.e., in many starting and stopping operations. The fan blades of the ATR, unlike those of ordinary aircraft, must withstand operation in an ultrahigh temperature environment. Therefore, the properties for environmental resistance required of them include high creep strength and oxidation resistance.

The mechanical properties required of the turbine blades, which are also rotary engine parts, are similar to those required of the abovementioned fan. However, since they come in contact with liquid hydrogen during operation, their brittleness against hydrogen also constitutes a factor to be considered with respect to their environmental resistance.

The intake is a static part to which the application of a functionally gradient material is being studied. The specific strength required of it is lower than that of rotary parts. Since it has a relatively simple shape (it is a thin plate formed with a large radius of curvature), the temperature and thermal stress distribution in the direction of plate thickness changes linearly. It is thought to be a suitable type of part for the use of functionally gradient material.

There will be many hurdles to be cleared before functionally gradient materials can be applied to such rotary parts as the fan, turbine blades, and the disk. The materials must have high specific strength. With the parts having complicated shapes, their thermal stress profiles will be complex and will vary as the engine is started and stopped. Therefore, many problems will have to be solved with regard to material design, forming and material strength evaluation.

At the stage of experimental parts manufacture, it will be necessary to evaluate parts workability and joinability and to test the parts in other respects by simulating their shapes and loads. The important tests to be conducted at the stage of practical use will include destruction tests to evaluate parts reliability and evaluation tests to verify the space resistance of the engine.

Problems With Exposed-to-Plasma Devices

43067606c Tokyo KEISHA KINO ZAIRYO KENKYUKAI in Japanese 1 Jul 88 pp 7-8a

[Article by Masahiro Seki, Japan Atomic Energy Research Institute: "Fusion Reactor Components Exposed to Plasma"]

[Text] Introduction

Fusion reactors are regarded as the next-generation nuclear systems coming after large-scale plasma confinement systems such as the JT-60, JET, and TFTR now in service. While these existing systems are aimed at achieving critical conditions using hydrogen or a deuterium plasma, fusion reactors are, as the name implies, intended to confine a combustion plasma along with the deuterium (D) and tritium (T). This article will focus on the tokamak-type fusion reactor among various types of plasma confinement systems. It goes without saying that the ultimate goal of fusion reactor development is to build power reactors for use in power generation. In the present stage, however, the principal research target in this area is to build an experimental reactor that can be used to confine a combustion plasma and attain self-igniting conditions. This experimental reactor is often referred to as the next-phase large-scale reactor system in the sense that it is expected to be the future system coming after existing large-scale systems such as the JT-60. In dealing with the next-phase large-scale reactor system in this article, the author will 1) explain the various types of load to which the exposed-to-plasma devices of the system--in particular, their surfaces--are subjected due to the presence of a plasma; 2) touch on the current status of relevant device design and research; and 3) discuss future tasks to be tackled, mainly regarding requirements to be satisfied in material development. The exposed-to-plasma devices literally refer to those devices directly exposed to plasma in a fusion reactor. Among them, the first wall, the limiter, and the diverter are the principal ones.

Fusion Reactor Composition and Environment for Exposed-to-Plasma Devices-- Loads on Exposed-to-Plasma Devices Caused by Plasma

Figure 1 shows a sectional view of the next-phase large-scale reactor system currently being designed mainly at the Japan Atomic Energy Research Institute. The system is designed to generate α particles of 5 MeV and neutrons of 14.1 MeV when DT reaction occurs in the plasma present in the central part of the system. The α particles heat the plasma itself, then

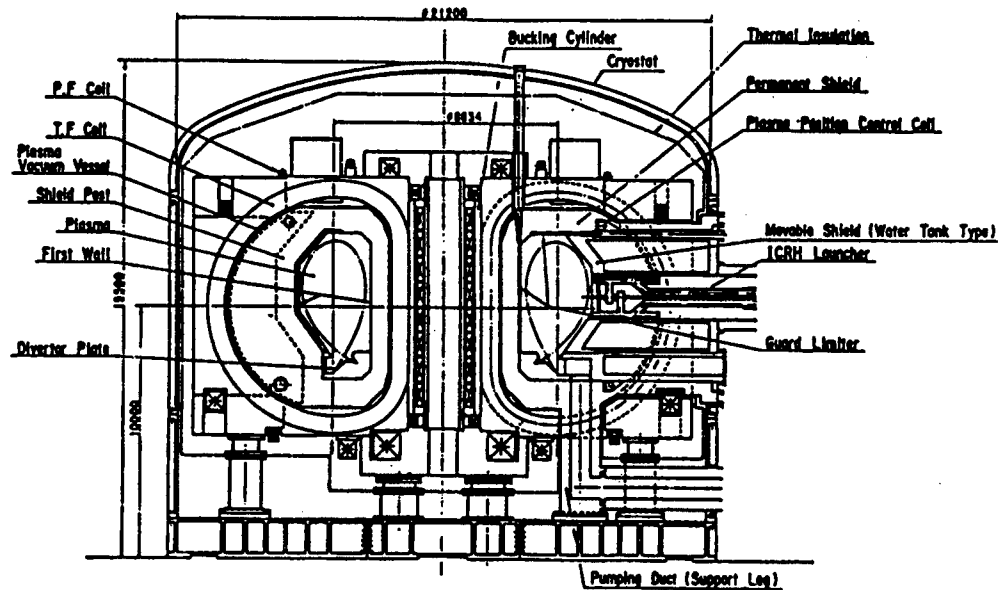


Figure 1. Sectional View of Next-Phase Large-Scale Reactor System Designed by Japan Atomic Energy Research Institute

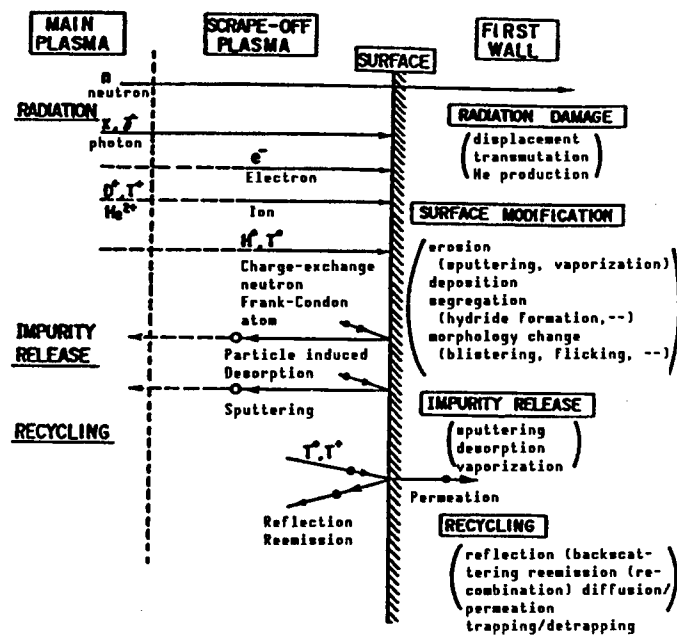


Figure 2. Interactions Between Plasma and Wall

become surface thermal loads on the surfaces of exposed-to-plasma devices. The neutrons cause volume heat generation in device materials. At the same time as the exposed-to-plasma devices are subjected to thermal loads, they are heavily irradiated with high-energy neutrons. Furthermore, the first wall is struck by plasma-constituting particles which have been neutralized

through charge exchange, whereas the diverter surface is hit by the charged particles coming in along the lines of magnetic force. As can be seen, the surfaces of the exposed-to-plasma devices are subjected to high thermal, particle, and neutron loads attributable to the plasma. The phenomena that may occur as interactions between the exposed-to-plasma device wall and the plasma are shown in Figure 2.

Device materials suffer notable property deterioration due to neutrons. Their surface is damaged by the sputtering of neutrons or charged particles. The thermal load applied to device materials generates high thermal stress in them. The estimated values of particle loads expected to be generated in the next-phase large-scale reactor system are listed in Table 1. These so-called normal loads are applied to the surfaces of the exposed-to-plasma devices while the plasma is burning in a normal state. When the plasma abruptly disappears in an abnormal state, that is, when a plasma disruption occurs, the huge plasma energy is instantaneously released against the exposed-to-plasma devices, causing the surfaces of the devices to be subjected to remarkably high pulses of thermal load. As a result, melting and evaporation takes place on the wall surface, damaging the wall surface. The wall surface may even be cracked or broken due to the thermal shock applied.

Table 1. Particle Loads in Next-Phase Large-Scale Reactor System

Diverter	
Average temperature of electrons	30 eV
Average energy of ions	135 eV
Composition of ions	47.5% D, 47.5% T, 5% He
Peak ion flux normal to diverter plates	
Outboard	$0.11 \times 10^{24}/\text{m}^2\text{s}$
Inboard	$0.11 \times 10^{24}/\text{m}^2\text{s}$
First wall	
Energy of ions	60 - 200 eV
Composition of ions	50% D, 50% T
Particle flux	$fr_0 \exp(-Z/\lambda)$
	$r_0: 1 \times 10^{22}/\text{m}^2\text{s}$
	$\lambda: 20 \text{ cm}$
	$Z: \text{coordinate along poloidal wall}$
	$f: \text{peaking factor 2}$

The estimated magnitudes of thermal load generated at plasma disruption can be seen in Figure 3, which shows the relationships between thermal fluxes moving toward the wall surface and thermal pulse duration. It can be seen that the thermal flux generated at plasma disruption can be as intensive as $10^3 \text{ MW}/\text{m}^2$, with the pulse duration being as short as 0.1-10 ms. The normal thermal load in the next-phase large-scale reactor system is estimated at about $2 \text{ MW}/\text{m}^2$ for the diverter and about $0.2 \text{ MW}/\text{m}^2$ for the first wall. If at the time of plasma disruption the plasma completely loses its thermal energy as well as its magnetic energy, the plasma current will disappear,

including an eddy current in the device, and as a result, allowing the generation of a strong electromagnetic force due to the interaction between the eddy current and a toroidal magnetic field. As the magnitude of this electromagnetic force is dependent on the device design, it is important to devise a means to deal with this force.

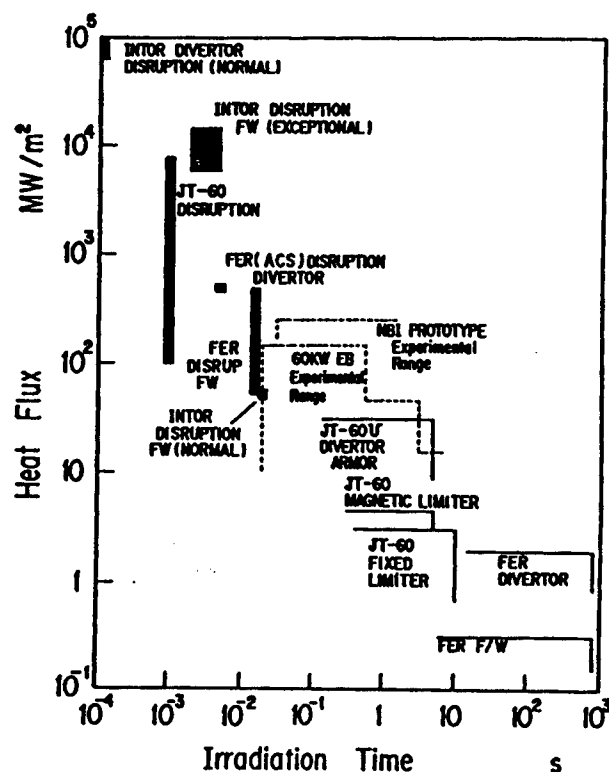


Figure 3. Thermal Loads in Fusion Reactors

Current Status of Design and Research

As discussed above, exposed-to-plasma devices that are to be incorporated in a fusion reactor are subjected to heavy loads. It is therefore necessary to design them in such a way that they have a reasonable length of service life during which they can withstand the loads attributable to the plasma. One of the problems currently regarded as important in this respect is how to deal with the high-temperature load generated at plasma disruption. In the next-phase large-scale reactor system FER shown in Figure 1, a guard limiter is attached to the inner first wall where the thermal load generated at plasma disruption is thought to concentrate so that it can deal with most of the thermal load. The guard limiter expected to be exposed to intensive thermal loads can be removed easily for replacement by lifting it straight up. The normal thermal load on the guard limiter is estimated at 0.2 MW/m², whereas the thermal load to which it is subjected at plasma disruption is estimated at 480 MW/m² in magnitude and 15 ms in duration. The guard limiter has a cooling structure made of stainless steel covered with brazed graphite tiles for protection against thermal shock. According to the results of

thermal analysis, the graphite tile temperature rises to about 3,600°C at plasma disruption. From this, it is estimated that the graphite tiles will suffer a loss due to sublimation of 36 μm per disruption.

Generally, heat conduction analysis codes that can be used to analyze phase changes are used for this type of thermal analysis. According to the results of disruption thermal load simulation tests recently conducted, when graphite is strongly heated, its fine particles sputter, inflicting damage far more severe than that estimated by calculation on its surface. So this phenomenon must be analyzed further by means of additional experiments and study in order eventually to create an appropriate analysis model and enhance the performance of analytical calculation codes.

The guard limiter to be subjected to the strong thermal load described above is made of a composite material comprised of graphite and stainless steel joined together. For the diverter plate to be subjected to heavy particle and thermal loads, it has been proposed to use a structure with tungsten as the surface material to minimize the damage by sputtering due to particle loads and with copper as a heat sink with high thermal conductivity. The use of tungsten as the surface material requires the plasma temperature in the diverter chamber to be low enough to permit the self-sputtering coefficient of tungsten to remain smaller than 1. For the next-phase large-scale reactor system being developed, many proposals have been put forward to use joined structural materials designed to have different functions performed by different materials. To introduce joined materials in the new reactor system, it is necessary to solve such problems as how to join different materials and how to enable the material joints to stay in good condition. In collaboration with private enterprises, the Japan Atomic Energy Research Institute is conducting research on various problems, including fabricability, regarding such joined materials as tungsten-copper and graphite-stainless steel. The problems to be solved before joined materials can be adopted as surface materials for exposed-to-plasma devices are shown in Figure 4.

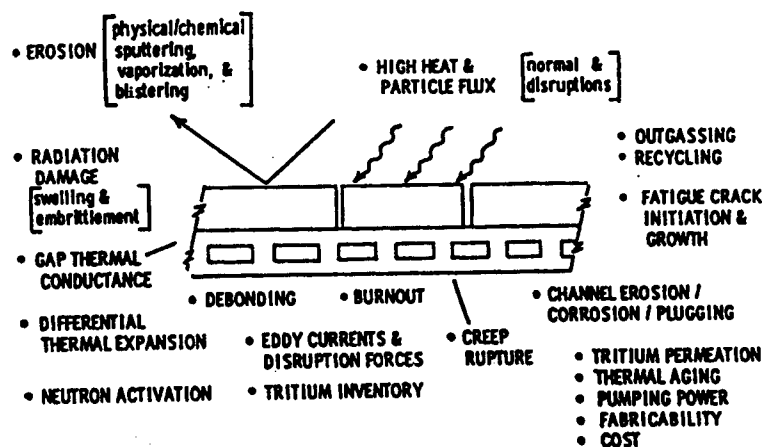


Figure 4. Main Research Targets Regarding Exposed-to-Plasma Devices

Future Tasks

As has been discussed, the exposed-to-plasma devices to be incorporated in a fusion reactor are subjected to composite loads. With regard to the effects of neutron irradiation on stainless steel to be used as a structural material, study is being positively promoted utilizing a fission reactor. However, when it comes to neutrons with energy as high as 14 MeV, there is almost no data on the effect of this on materials. So it is hoped that henceforth research will be promoted in this area. Among the various types of stress applied to the device surface, thermal stress is predominant. With the present design of the first wall, material wear caused by sputtering due to neutron particles or by evaporation due to the thermal load generated at plasma disruption is unavoidable. Permitting the normal thermal load to generate greater thermal stress means increasing the wall thickness in anticipation of such material loss. Therefore, it is hoped that materials featuring low thermal-stress generation will be developed. For the device design, it is also important to establish design criteria for the materials to be subjected to special loads such as those generated at plasma disruption.

Thermoelasticity Estimation Model for Polyphase Mixed Systems

43067606d Tokyo KEISHA KINO ZAIRYO KENKYUKAI in Japanese 1 Jul 88 pp 9-14

[Article by Kenji Wakasima, et al., Fine Engineering Laboratory of Tokyo Institute of Technology: "Thermoelasticity Estimation Model for Polyphase Mixed Systems"]

[Text] 1. Introduction

When designing functionally gradient materials (FGMs) with the main aim of achieving thermal stress relaxation, data on the thermal as well as mechanical properties of heterogeneous systems including, for example, ceramic-metal composites are required. Among the various kinds of data on material properties, the elastic constant, the coefficient of thermal expansion, and the thermal conductivity are indispensable in analyzing the thermal stress in any FGM. If the FGM to be designed is to be used in an unsteady state, heat-specific data will also be required to analyze problems related to unsteady-state heat conduction.¹

These "macroscopic" properties of mixed systems vary in complex ways as a result of the effect of various "microscopic" factors. One of the microscopic factors is the constitutive material mixing ratios (ratios among constitutive phases). This factor alone cannot uniquely define the macroscopic properties of a mixed system; for this, it is also necessary to study the geometric factors that define in detail the microstructure of the mixed system. Take a two-phase system comprised of a matrix of material A in which material B is dispersed as a disperse phase, for example. The macroscopic properties of this mixed system are affected by the shape and orientation of disperse phase B. The properties of many ceramic-metal systems are affected by pores. The effects of pores on their elastic constants are particularly great. For ceramic-metal systems, pores should be regarded as virtually constituting a phase. Therefore, to design a ceramic-metal system, not only the porosity but also the data on pore shapes must be taken into account. Because analysis of the properties of mixed systems requires complex factors to be taken into account, data on the macroscopic properties of mixed systems that has been obtained through actual measurement can currently be found only in a limited amount of literature. So the present situation is highly inadequate in terms of both quality and quantity from the viewpoint of systematic promotion of the designing of FGMs.

On the other hand, it is possible to estimate theoretically the macroscopic properties of mixed systems based on information on their microstructural factors including data on the properties of constitutive materials and mixing ratios (volume fractions) using a micromechanical approach based on a specific continuum theory.²⁻⁴ Once the rules (rules of mixing) governing the macroscopic properties of mixed systems with different microstructures are made clear, the freedom of FGM design will be notably enhanced and the systematic classification and organization of data obtained through actual measurement will be facilitated.

Taking into account the diversity of the microstructures of mixed systems, this article will introduce a model designed for use in estimating the elastic constants and thermal expansion coefficients among the macroscopic properties of mixed systems.

2. Microstructure Model of Polyphase Mixed Systems

Actual polyphase mixed systems have various microstructures. These systems can be geometrically simplified by extracting the characteristics of their microstructures. In the present study, a model, as shown in Figure 1, of polyphase mixed systems comprised of a matrix and disperse phases will be discussed. The assumptions made for modeling are: 1) each polyphase mixed system contains N kinds of disperse phases; 2) each disperse phase consists of a set of congruent ellipsoids of revolution; 3) these ellipsoids are oriented with their main axes (axes of revolution) oriented in a certain direction, but they are arranged in a random spatial distribution (configuration) in a macroscopically uniform manner; and 4) the ellipsoids constituting different kinds of disperse phases generally differ in shape and orientation. Based on this model, the microstructure of a mixed system can be described by the following factors:

- Kind of disperse phase: n ($= 1, 2, \dots, N$)
- Disperse phase shape: $\eta^{(n)}$ ($= c^{(n)}/a^{(n)}$)
- Disperse phase orientation: $\theta^{(n)}$ $\phi^{(n)}$
- Disperse phase volume factor: $f^{(n)}$

In the above expressions, $\eta^{(n)}$ represents the axis ratio of an ellipsoid and $\theta^{(n)}$ and $\phi^{(n)}$ both represent Eulerian angles of a rotational axis (Figure 1).

3. Derivation of Constitutive Equations (Stress-Strain Relationships)

In this section, thermal elasticity constitutive equations will be derived by micromechanically analyzing the polyphase mixed system model shown in Figure 1. The strain product of the thermal expansion coefficient and temperature change) created in a material due to thermal expansion is inelastic and free of stress. This inelastic strain is generally referred to as proper strain.⁴ The strain involved in phase transformation and that caused by plastic deformation fall in the category of proper strain. In the following, constitutive equations for mixed systems with inelastic strain will be derived using a general method without regard to the type of proper strain.

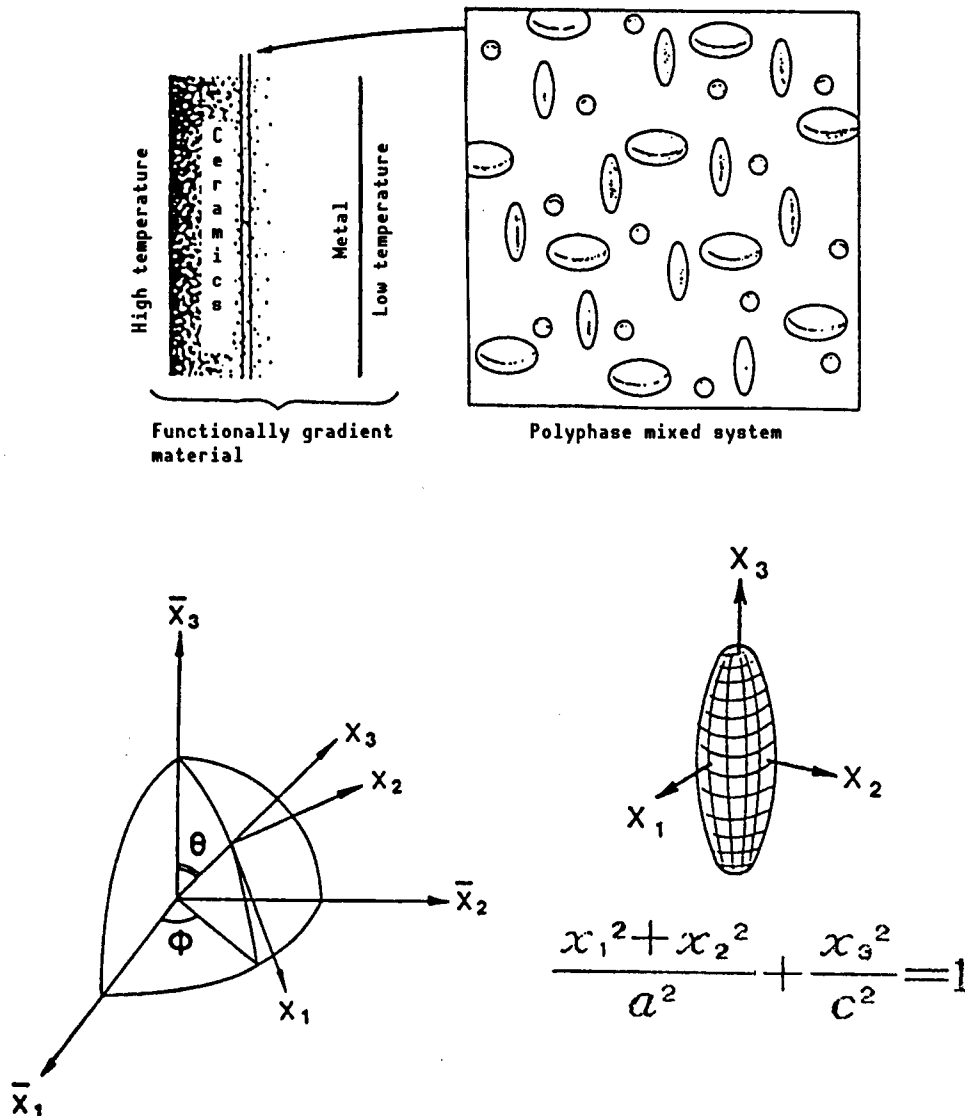


Figure 1. Polyphase Mixed System Microstructure Model

First, from the standpoint of continuum mechanics, the representative volume element (RVE) V_R maintaining the microstructural state of a polyphase mixed system will be discussed. Assuming that the surface of S_R of V_R (unit volume; $V_R = 1$) is subjected to the surface force T_i^o :

$$T_i^o = \sigma_{ij}^o n_j \quad (1)$$

In the above equation, σ_{ij}^o is a constant stress uniformly distributed in an object and n_i is a unit normal vector on the object surface S_R . As for the repetition index, the summation rule is to be applied. σ_{ij}^o is the stress generated in the object V_R with the elastic constant remaining the same in the entire part of the object. Equation (1) prescribes that, when the object is subjected to an external force, stress as described above is generated in it. In reality, however, the object V_R is an elastic

heterogeneous object comprised of two or more phases with different elastic constants, so the stress generated in it is microscopically uneven. Let us define this microscopically uneven stress as σ'_{ij} . Obviously, the boundary condition $\sigma'_{ij}n_j = T^0_i$ must be met on the object surface S_R . Also, based on the condition of static equilibrium, $\sigma'_{ij,j} = 0$. $(\cdot)_j$ represents the partial differential in coordinate component x_j . From these conditions, the following result can be derived:

$$\bar{\sigma}'_{ij} = \int \sigma'_{ij} dV = \sigma^0_{ij} \quad (2)$$

The region of the volume integral and that of the surface integral are V_R and S_R , respectively.

Assuming that each constitutive phase is accompanied by a constant proper strain $\epsilon^{*(n)}_{ij}$, this proper strain will result in creating a stress σ''_{ij} in the object V_R . Since this stress satisfies the condition of $\sigma''_{ij}n_j = 0$ on S_R and $\sigma''_{ij,j} = 0$ on V_R ,

$$\bar{\sigma}''_{ij} = \int \sigma''_{ij} dV = 0 \quad (3)$$

From the above, it can be seen that the macroscopic stress $\bar{\sigma}_{ij}$ in a polyphase mixed system defined as the volume average of the microscopic stress $(\sigma'_{ij} + \sigma''_{ij})$ over the entire part of the object V_R is equal to σ^0_{ij} , i.e., $(\bar{\sigma}_{ij} = \sigma^0_{ij})$.

The constitutive equations for a mixed system are none other than equations expressing the relationships between the microscopic stress $\bar{\sigma}_{ij}$ and macroscopic strain $\bar{\epsilon}_{ij}$ in the mixed system.

When a thermodynamic potential of a system is represented by Φ ,

$$\bar{\epsilon}_{ij} = -(\partial\Phi/\partial\bar{\sigma}_{ij}) \quad (4)$$

Based on this relationship, a constitutive equation can be derived through the following process: Φ is given by the equation,

$$\Phi = (1/2)\int(\sigma'_{ij} + \sigma''_{ij})(\epsilon'_{ij}) dV - \int T^0_i(u'_i + u''_i) dS \quad (5)$$

Where u'_i and u''_i are displacements, ϵ'_{ij} is the elastic strain due to stress σ'_{ij} and ϵ''_{ij} is the elastic strain due to stress σ''_{ij} ;

$$(1/2)(u'_{i,j} + u'_{j,i}) = \epsilon'_{ij} \quad (6)$$

$$(1/2)(u''_{i,j} + u''_{j,i}) = \epsilon''_{ij} + \epsilon'_{ij} \quad (7)$$

Equation (1) can be transformed as follows:

$$\begin{aligned} \Phi = & [(1/2)\int\sigma'_{ij}\epsilon'_{ij}dV = \int T^0_i u'_i dS] \\ & + (1/2)\int\sigma''_{ij}\epsilon''_{ij}dV \\ & - \int T^0_i u''_i dS \\ & + (1/2)\int(\sigma'_{ij}\epsilon''_{ij} + \sigma''_{ij}\epsilon'_{ij}) dV \end{aligned} \quad (8)$$

Through some calculations, each term of the above equation can be rewritten as follows:

$$\text{1st term} = -(1/2) \bar{\sigma}_{ij} \sum f^{(n)} M_{ijkl}^{(n)} \bar{\sigma}'_{kl} \quad (9)$$

$$\text{2d term} = -(1/2) \sum f^{(n)} \epsilon^{*(n)}_{ij} \bar{\sigma}'_{ij} \quad (10)$$

$$\text{3d term} = - \sum f^{(n)} \epsilon^{*(n)}_{ij} \bar{\sigma}'_{ij} \quad (11)$$

$$\text{4th term} = 0 \quad (12)$$

In the above equations, $M_{ijkl}^{(n)}$ is the elastic compliance constant of a constitutive phase and $\bar{\sigma}'_{ij}$ is the average of σ'_{ij} in the constitutive phase. The latter can be expressed as follows:

$$\bar{\sigma}'_{ij} = B^{(n)}_{ijkl} \bar{\sigma}_{kl} \quad (13)$$

Since $\sum f^{(n)} \bar{\sigma}'_{ij} = \bar{\sigma}_{ij}$, $B^{(n)}_{ijkl}$ must satisfy the following condition:

$$\sum f^{(n)} B^{(n)}_{ijkl} = I_{ijkl} \quad (14)$$

(I_{ijkl} is the fourth-order unit tensor; when Kronecker's delta is represented by δ_{ij} , $I_{ijkl} = (1/2)(\delta_{ik}\delta_{jl} + \delta_{il}\delta_{jk})$). $\bar{\sigma}^{(n)}_{ij}$ is the average of $\sigma^{(n)}_{ij}$ in a constitutive phase. Obviously, this is unrelated to $\bar{\sigma}_{ij}$. Therefore, from equation (4),

$$\bar{\epsilon}_{ij} = \sum f^{(n)} M^{(n)}_{ijmn} B^{(n)}_{mnkl} \bar{\sigma}_{kl} + \sum f^{(n)} \epsilon^{*(n)}_{kl} B^{(n)}_{kl ij} \quad (15)$$

The first and second terms of this constitutive equation represent the elastic and inelastic parts, respectively. This equation can be converted into a thermoelastic constitutive equation by expressing the proper strain of the constitutive phase as follows:

$$\epsilon^{*(n)}_{ij} = \alpha^{(n)}_{ij} \theta \quad (16)$$

In the above equation, $\alpha^{(n)}_{ij}$ is the thermal expansion coefficient tensor of the constitutive phase and θ is the temperature change ($\theta = T - T_0$) from the reference temperature T_0 . Therefore, when the elastic compliance tensor of the mixed system is represented by M_{ijkl} and the thermal expansion coefficient is represented by α_{ij} ,

$$\bar{\epsilon}_{ij} = M_{ijkl} \bar{\sigma}_{kl} + \alpha_{ij} \theta \quad (17)$$

$$M_{ijkl} = \sum f^{(n)} M^{(n)}_{ijmn} B^{(n)}_{mnkl} \quad (18)$$

$$\alpha_{ij} = \sum f^{(n)} \alpha^{(n)}_{kl} B^{(n)}_{kl ij} \quad (19)$$

The process of deriving the thermoelastic constitutive equations for a mixed system by a micromechanical approach has been explained. The above constitutive equations are only formal expressions. To utilize them, the contents of $B^{(n)}_{ijkl}$ must be made clear. This tensor, as seen from equation (13), is a constant expressing the degree of concentration of the average of the external stress, with respect to the macroscopic stress (load

stress), applied to each constitutive phase of a mixed system, and it is referred to as the phase stress concentration-factor tensor. This constant is dependent on the foregoing factors (Figure 1) defining the microstructure

of a mixed system. It can be expressed as shown below, although the process of deriving the following equation is not explained here⁶:

$$B^{(n)}_{ijkl} = L^{(0)}_{ijmn} R^{(n)}_{mnpq} \langle R_{pqrs} \rangle^{-1} M^{(0)}_{rskl} \quad (20)$$

In the above equation, $L^{(0)}_{ijkl} = (M^{(0)}_{ijkl})^{-1}$ is the elastic stiffness of the matrix ($n = 0$). $R^{(n)}_{ijkl}$ and $\langle R_{ijkl} \rangle$ have been defined as shown below, respectively.

$$R^{(n)}_{ijkl} = I_{ijkl} - (S^{(n)}_{ijmn} - I_{ijmn}) \times \\ (L^{(0)}_{mnpq} + L^{(n,0)}_{mnrs} S^{(n)}_{rspq})^{-1} L^{(n,0)}_{pqkl} \quad (21)$$

$$\langle R_{ijkl} \rangle = \sum f^{(n)} R^{(n)}_{ijkl} \quad (22)$$

For the above equations, $L^{(n,0)}_{ijkl} = L^{(n)}_{ijkl} - L^{(0)}_{ijkl}$. $S^{(n)}_{ijkl}$ included in equation (21) is the Eshelby tensor. It is a constant dependent on the axis ratio $\eta^{(n)}$ and orientation angles $\theta^{(n)}$ and $\phi^{(n)}$ of an ellipsoid and the elastic constant of the matrix.⁷ The matrix is an isotropic elastic body. When the target disperse phase is spherical ($\eta = 1$), $S_{1111} = S_{2222} = S_{3333} = (7-5\nu)/[15(1-\nu)]$, $S_{1122} = S_{2233} = S_{3311} = -(1-5\nu)/[15(1-\nu)]$, $S_{1212} = S_{2323} = S_{3131} = (4-5\nu)/[15(1-\nu)]$, and $S_{ijkl} = 0$; where ν represents the Poisson's ratio. This can be calculated with ease even if the axis ratio η is arbitrarily set, though the results are not shown here.

4. Numerical Computation Program Composition, Utilization

We have created a numerical computation program in FORTRAN for use in calculating the elastic constants and thermal expansion coefficients for polyphase mixed systems according to the above derived equations. This program consists of an input section, a numerical computation section, and an output section. The input and output sections, which will be of most interest from the user's point of view, are explained in the following:

Input section: In this section of the program, the target polyphase mixed system is specified, and information on the microstructure of the mixed system and data on the properties of the constitutive phases are input. The processing performed by this input section is described in the following:

(1) The matrix material is specified and its elastic constant and thermal expansion coefficient are input. This input operation is performed by means of calling the corresponding material data file from a database. This program has been created on the assumption that the matrix is always selected from isotropic materials. Therefore, the property data to be input is comprised of three items, i.e., Young's modulus E , Poisson's ratio ν , and coefficient of linear expansion α .

(2) The number of disperse phases contained in the target mixed system (i.e., the value of N) is specified. If the target mixed system has pores, they are classified by type and are regarded in this program as constituting constitutive phases.

(3) Each of the disperse phases ($n = 1, 2, \dots, N$) is specified as an isotropic body or an axis-symmetrical anisotropic body (intrasurface isotropic body). Next, the elastic constant and the thermal expansion coefficient for each disperse phase are input. Like the operation described in (1), this operation also constitutes the calling of a data file. In this case, however, the operation format differs depending on whether the material is to be treated as an isotropic body or an anisotropic body. Therefore, two different data files must be prepared for the same material. For an isotropic body, three properties are input: Young's modulus E , Poisson's ratio ν , and coefficient of linear expansion α . For an anisotropic body, five kinds of elastic constants--Young's modulus E_T and E_L , Poisson's ratios ν_{TL} and ν_{TT} , and modulus of rigidity G_{LT} --and two thermal expansion coefficients, α_T and α_L , are required. In these symbols, L represents an axial direction and T represents a lateral direction perpendicular to the direction of L . The property of pores may be expressed, for example, as $E = \nu = \alpha = 0$.

(4) For each disperse phase, orientation angles $\theta^{(n)}$ and $\phi^{(n)}$, aspect ratio $\eta^{(n)}$, and volume ratio $f^{(n)}$ are specified.

Output section: The values of the elastic constant and thermal expansion coefficient obtained through numeric computation carried out using the abovementioned input data are output in matrix form. This arrangement in programming has been made as a result of taking into account that, even if all the constitutive phases comprise isotropic bodies, the microstructure anisotropy causes the material properties to show anisotropy. For the conversion of matrices into Young's modulus E , Poisson's ratio ν , and modulus of rigidity G , see Table 1.

Table 1. Elastic Compliance Matrices for Orthogonal Anisotropic Bodies

$1/E_1$	$-\nu_{21}/E_2$	$-\nu_{31}/E_3$	0	0	0
$-\nu_{12}/E_1$	$1/E_2$	$-\nu_{32}/E_3$	0	0	0
$-\nu_{13}/E_1$	$-\nu_{23}/E_2$	$1/E_3$	0	0	0
0	0	0	$1/G_{23}$	0	0
0	0	0	0	$1/G_{31}$	0
0	0	0	0	0	$1/G_{12}$

Note: Poisson's ratio $\nu_{ij} = -\epsilon_j/\epsilon_i$, where i represents the direction of the tension/compression axis, and j represents the lateral perpendicular direction.

5. Conclusion

In this paper mixing rules concerning the elastic constants and thermal expansion coefficients of polyphase mixed systems have been derived using a micromechanical approach, and the computation program created based on the

derived mixing rules has been outlined. The research conducted so far has dealt mainly with particle- or fiber-reinforced "composite materials." In research in that area, it is assumed that disperse phases are, in almost all cases, either spherical or cylindrical (with an infinite length). In addition, when disperse phases are assumed to be cylindrical, in most cases they are assumed to be unidirectionally oriented.²⁻⁴ Even though the microstructure model created in the present study concerns polyphase mixed systems consisting of a matrix and disperse phases, it should be noted that the applicability of the model is remarkably extensive. The mixing rules derived are compatible with other mixing rules introduced so far. They comply, for example, with Hashin-Shtrikman's bounds²⁻⁴ of elastic constants --a condition to be met by macroscopically isotropic polyphase mixed systems with arbitrary microstructures (even the distinction between the matrix and disperse phases need not be made). Furthermore, they are able to provide a solution to the problem of what microstructural states the upper and lower bounds of elastic constants will correspond to. More detailed discussion in this regard will be left to another time.

References

1. Report on the "Survey of fundamental technology for obtaining new functions and achieving thermal stress relaxation through material complexation" compiled by the Mitsubishi Research Institute Inc. under the government fund for science and technology promotion adjustment for FY 1986 (May 1987).
2. Z. Hashin, APPL. MECH. REV., Vol 17, 1964, p 1.
3. Ibid., in "Mechanics of Composite Materials" (Edited by W. Wendt, et al.), Pergamon Press, Oxford, 1967, p 201.
4. R.M. Christensen, "Mechanics of Composite Materials," John Wiley & Sons, New York, 1979.
5. T. Mura, "Micromechanics of Defects in Solids" (2d Revised Ed.), Martinus Nijhoff Publishers, Dordrecht, 1987.
6. K. Wakashima and T. Mori, in "Constitutive Relations and Their Physical Basis," (Proc. of the 8th RISO Int. Sym. on Met. & Mater. Sci.), RISO National Laboratory, Roskilde, Denmark, 1987, p 543.
7. J.D. Eshelby, PROC. ROY. SOC., Vol A241, 1957, p 376.
8. Ibid., Vol A252, 1959, p 561.

Functionally Gradient Material Design Aid System

43067606e Tokyo KEISHA KINO ZAIRYO KENKYUKAI in Japanese 1 Jul 88 pp 15-18

[Article by Tooru Hirano, CAE Center, Daikin Industries, Ltd.: "Development of Functionally Gradient Material Design Aid System"]

[Text] 1. Introduction

For the development of space structures and fusion reactors being pursued in recent years, the development and selection of ultraheat-resistant materials has assumed great importance. In fact, studies are being positively promoted in this area. Japan has a plan to develop a space shuttle through joint efforts exerted on a national scale over a period extending into the 21st century, and this calls for the development of new materials with heat resistance higher than that of conventional composite materials. In connection with this need, the author, et al., proposed the use of functionally gradient materials to be produced through continuous multidimensional control of their mixing ratio among different types of components such as ceramics and metals. Subsequently, we have conducted fundamental research and synthesis experiments and we have been studying a design aid system.^{1,2} This design aid system is aimed at enabling structural member materials to obtain the function of thermal stress relaxation. It can be said that the design of material functions and structures is integrated in this design aids system. The conventional concepts of material design and databases for use in material design are based on the assumption that the materials to be handled are generally homogeneous. In the case of functionally gradient materials, however, their heterogeneity is positively made use of. Therefore, design aid systems to be used in designing functionally gradient materials should be capable of numerical simulations and should employ knowledge engineering techniques.

2. Structure of Design Aid System

In designing a functionally gradient material, it is necessary to adopt an inverse design approach (Figure 1). In this approach, first, the material shape and interface conditions to be achieved are determined according to the intended application, then two or more synthesizable combinations of materials are selected and the parameters defining their mixing ratio gradient profile are tentatively determined. Next, the selected materials are analyzed as to thermal conduction and stress using a material property

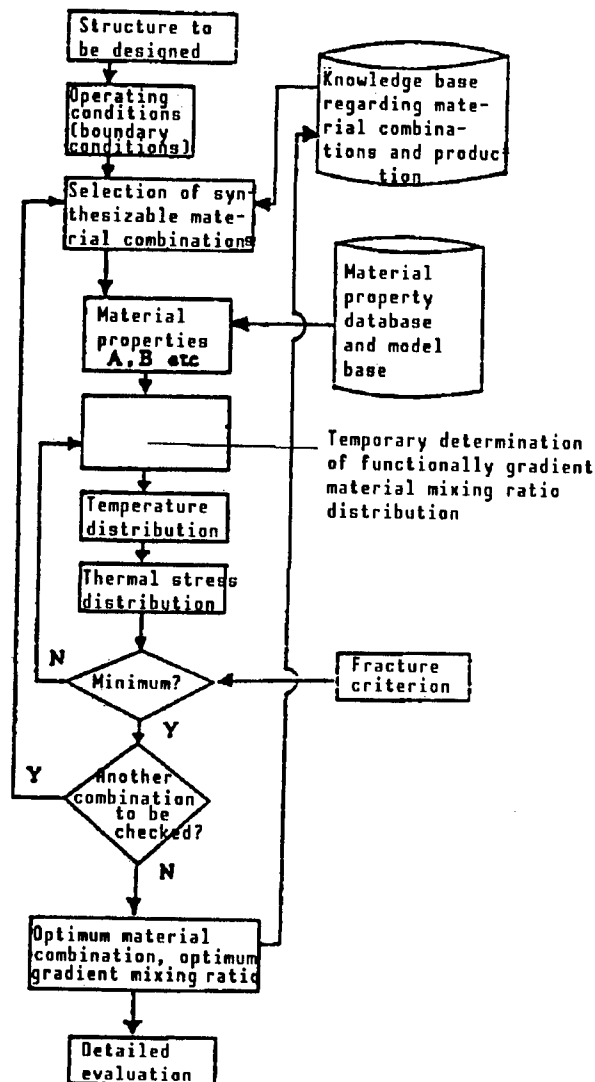


Figure 1. Functional Material Inverse Design Process

database. By carrying out this analysis for various gradient profile parameters and different material combinations, the gradient profile parameters and the material combination that will minimize the generation of thermal stress are decided on. In this process, it becomes necessary to use a knowledge base containing various control conditions regarding material combinations and composite material production as well as a knowledge database capable of automatic interpolation or estimation to supplement discrete data points.

Figure 2 shows the basic architecture we have adopted for this design system. As shown, this basic architecture is comprised of a graphic engine that provides an interactive interface between this design aid system and material designers, a Prolog-based inference engine to be used to conduct

inference based on an expert knowledge base, and an analysis engine capable of repeatedly carrying out, for example, thermal stress analysis at high speed.^{3,6}

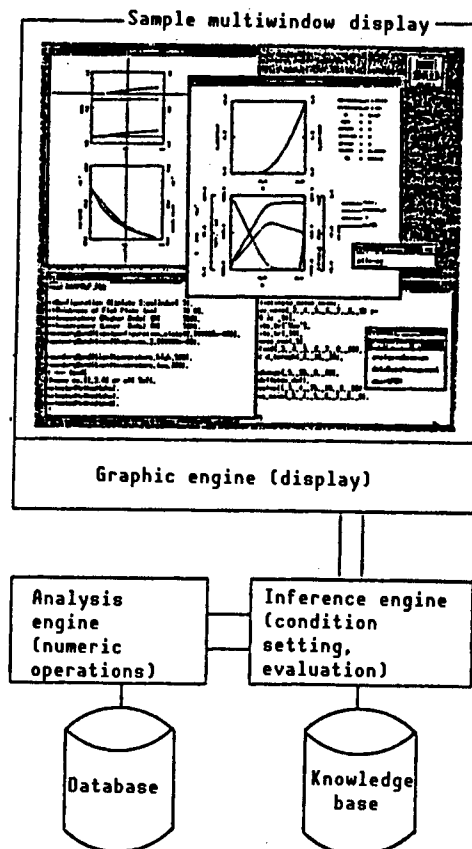








Figure 2. Functionally Gradient Material Design Aid System

Table 1. Mixing Rule Selection According to Microstructure

Phase arrangement in hypothesized layers Continuous phases Blue : phases White: Dispersed phases						
	Laminated	Fiber(1)	Fiber(2)	Thin Layer	Flake-like	Spherical Particle
Thermal conductivity λ	Harmonic average rule	Harmonic average rule	Linear complexation rule	Linear complexation rule	Kerner's mixing rule	Kerner's mixing rule
Coefficient of thermal expansion α	Rigidity modifying complexation rule	Rigidity modifying complexation rule	Linear complexation rule	Linear complexation rule	Eshelby's mixing rule	Kerner's or Turner's rule
Modulus of elasticity E, K, G	Linear complexation rule	Linear complexation rule	Harmonic average rule	Harmonic average rule	Eshelby's mixing rule	Kerner's mixing rule

This architecture enables utilization of the backtrack function incorporated in Prolog so that the search of the solution space regarding material combinations can be automated.^{4,5} The inference engine included in this design aid system has a knowledge base comprised, as outlined in Table 1, of the mixing rules concerning material properties such as thermal conductivity, the thermal expansion coefficient, and the modulus of elasticity for various microstructures of functionally gradient materials. This knowledge base also makes it possible to identify the mixing rule, according to which a nongradient (homogeneous) or gradient material is made up inversely from the measured values of its properties.^{4,5}

This analysis engine in its present state incorporates an infinite flat plate model and an infinite cylinder model only. Both models are designed to solve equations of thermal conductivity for functionally gradient materials whose compositions change continuously along the direction of their thickness and to estimate their thermal stress profile by analyzing the plane stress or strain expected to be generated in them. This analysis engine has been written in FORTRAN, enabling high-speed numeric operation.

3. Functionally Gradient Material Design Example

Figure 3 shows an example of the design, carried out using this design aid system, of a combustor material for a reusable rocket engine. The model used in designing the material is a cylinder with a 95 mm inner diameter and a 10 mm wall thickness. It was assumed that the cylinder would be heated to 1,500 K on its inner surface and 300 K on its outer surface. The functionally gradient material consequently designed is an optimum one from the viewpoint of preventing steep changes in the distribution of thermal stress in it. It is to be made of TiB_2/Cu --a metal-ceramic system on which synthesis experiments by the self-exothermic reaction method are being conducted.

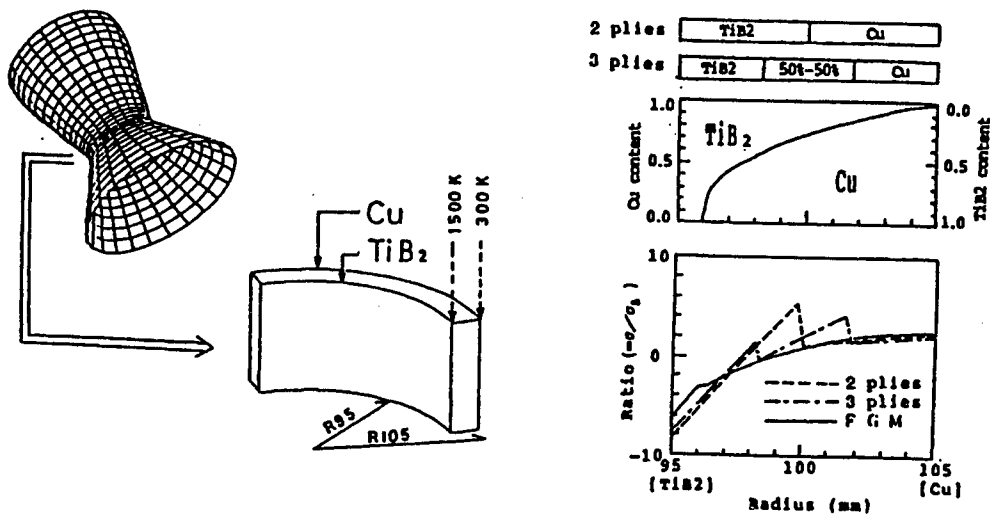


Figure 3. Rocket Engine Combustor Material Design
(a) Rocket engine combustor and analysis model
(b) Effect of functionally gradient material

In designing the combustor material, the mixing rules concerning its thermal conductivity and thermal expansion were identified based on the measurements of properties of the respective nongradient materials. Next, the microstructure of the target combustor material was determined based on the knowledge base outlined in Table 1, and a mixing rule concerning a modulus of elasticity that has not been measured was determined through inference. It is seen from Figure 3(b) that in a composite material consisting of a TiB_2 layer and a Cu layer, or comprised of three layers with an intermediate layer sandwiched between the abovementioned two layers, tensile stress is generated along the layer interfaces, posing the possibility of the layers being separated, whereas in functionally gradient material (FGM), the TiB_2 layer is subjected to compression only. It is therefore assumed that the FGM is more resistant to fracture than the layered composite material.

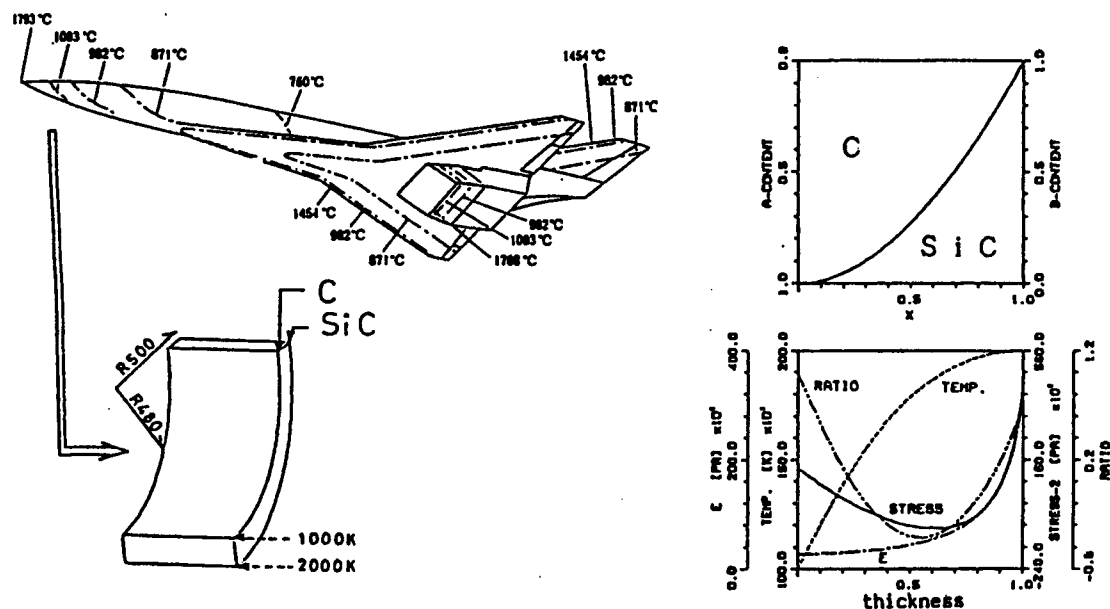


Figure 4. Space Shuttle Airframe Material Design
 (a) Space shuttle and analysis model
 (b) Gradient composite profile and internal status

We have also designed, as shown in Figure 4(a), a heat-insulating material for a space shuttle. The material designed is to comprise an SiC/C system to be synthesized by the chemical vapor deposition method. The mixing-ratio gradient profile parameters determined to be optimum varied depending on whether priority was attached to the minimization of the maximum specific stress (the ratio of stress to strength) or to that of the average density. As design criteria, we adopted the parameters estimated to be optimum for minimizing the average density based on the consideration that the material to be designed was for use in a spacecraft and therefore that it should be as light as possible (Figure 4(b)).

4. Future Prospects

In this expert system, we intend to improve and expand the knowledge base as well as the database to be used in designing functionally gradient materials. We also aim at incorporating the analysis engine into a special CPU and additionally at providing it with a multidimensional elastic-plastic analysis function.

References

1. T. Hirano, et al., "Inverse Approach for Designing Functionally Gradient Materials," lecture meeting on strength of materials held by the Institute of Mechanical Engineers of Japan, No 860-10, 1986, p 21.
2. Research and Development Bureau, Science and Technology Agency, "Report on a Survey of Fundamental Technology for Function Generation and Thermal Stress Relaxation Through Material Complexation," compiled under disbursement from the government's fund for science and technology promotion and adjustment for FY 1986.
3. T. Hirano, et al., "Fundamental Research on Application of Functionally Gradient Material to Rocket Combustor," 31st lecture meeting of Uchu Kagaku Rengokai [Space and Science Association], 1987, p 628.
4. Ibid., "Attempt To Use AI Approach for Inverse Problem Analysis," lecture meeting on strength of materials held by the Institute of Mechanical Engineers of Japan, No 870-12, 1987, p 20.
5. Ibid., "Multi-paradigm Expert System Architecture Based Upon the Inverse Design Concept," International Workshop on Artificial Intelligence for Industrial Applications, 25-27 May 1988, Hitachi, Japan.
6. Ibid., "A Study on a Functionally Gradient Material Design System for a Thrust Chamber," 16th International Symposium on Space Technology and Science, 22-27 May 1988, Sapporo, Japan.

Functionally Gradient It-TiN, Cr-CrN Composites

43067606f Tokyo KEISHA KINO ZAIRYO KENKYUKAI in Japanese 1 Jul 88 pp 19-23

[Article by Susumu Ikeno, National Research Institute for Metals: "Manufacture by PVD Method and Properties of Functionally Gradient It-TiN and Cr-CrN Composites"]

[Text] 1. Introduction

In the space-, aeronautics-, and nuclear power-related fields where ultrahigh-speed operation is performed involving ultrahigh temperature, composite materials consisting of metal with ceramics bonded or thermal-sprayed over their surface are in use. When they are exposed to high temperature, thermal stress is generated at the interfaces between the ceramic and the metal. This creates the possibility of their being broken or cracked at the interfaces. To avoid this problem, it is desirable to develop ceramic-metal composites having gradient composition profiles without any clear phase interface. In the present study, attention has been focused on two materials: titanium (It)--a metal important as an aircraft material--and chromium (Cr)--an important alloy element for the manufacture of heat-resistant materials. We also experimented in creating functionally gradient ceramics comprised of nitrides of the above two metals, i.e., Ti-TiN and Cr-CrN (the arrow indicates that the composition changes gradually). Before experimenting in creating these ceramics, we studied the properties of the respective nongradient ingredients. For the experimental ceramics creation, we used the HCD-type PVD process.

2. Ion Plating by HCD-Type PVD Process

Figure 1 shows the ion plating system used in our experiment. The vacuum chamber has an inner diameter of 600 mm and a volume of $1.5 \times 10^{-1} \text{ m}^3$. for film formation, the vacuum chamber is evacuated to a vacuum of $2 \times 10^{-3} \text{ Pa}$ and then an argon gas is introduced into the vacuum chamber via an HCD-type gun while a large current is made to flow at a low voltage between the HCD-type gun and the water-cooled copper crucible, causing the generation of argon plasma. This argon plasma melts the metal in the crucible, letting it evaporate. It also serves to ionize the metallic vapor. The ionization of the metallic vapor results in the tighter formation of a higher density film over a metal substrate set above the crucible. The evaporated film of a compound such as an oxide, carbide or nitride can be obtained by introducing the corresponding reaction gas into the ionized metallic vapor.

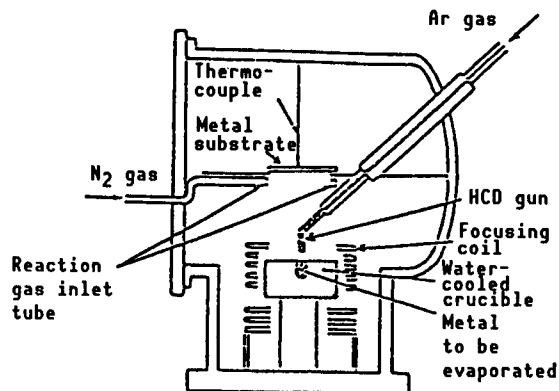


Figure 1. Ion Plating System

3. It-TiN Evaporated Films With Nongradient Composition and With Gradient Composition

3.1 It-TiN Evaporated Films With Nongradient Composition

Films of TiTiN with nongradient composition were created over stainless steel substrates (2 mm x 9 mm x 15 mm) by evaporating It at a constant rate (30 $\mu\text{m/hr}$) and introducing a nitrogen gas into the It vapor. This experiment was carried out with various flow rates of the nitrogen gas, i.e., at 0 cc/min (partial pressure: 0 Pa), 50 cc/min (3×10^{-3}), 100 cc/min (6×10^{-3}), 150 cc/min (9×10^{-3}), and 200 cc/min (1×10^{-2}). The structures and textures of the It-TiN films formed under the various conditions were examined by conducting crystal structure analysis using X-rays and elementary analysis using an EPMA (electron probe microanalyzer).

Figure 2 shows the X-ray diffraction intensity exhibited by the nongradient composition It-TiN films formed through evaporation. As shown, as the nitrogen gas flow rate was increased by steps, the evaporated film structure shifted from an It phase to an It-Ti₂N mixed phase, then to a Ti₂N-TiN mixed phase and to a TiN phase. The TiN phase resulted from a nitrogen gas flow rate of 150 cc/min or more.

3.2 It-TiN Evaporated Films With Gradient Composition

In another part of our experiment, we created a gradient composition film of It-TiN by changing the nitrogen gas flow rate at a certain rate during the It evaporation. Namely, the nitrogen gas flow rate was increased from 0 cc/min to 150 cc/min in 45 minutes at a certain rate (10/3 cc/min/min). The X-ray diffraction intensity exhibited by the film formed in this way is shown in Figure 3.

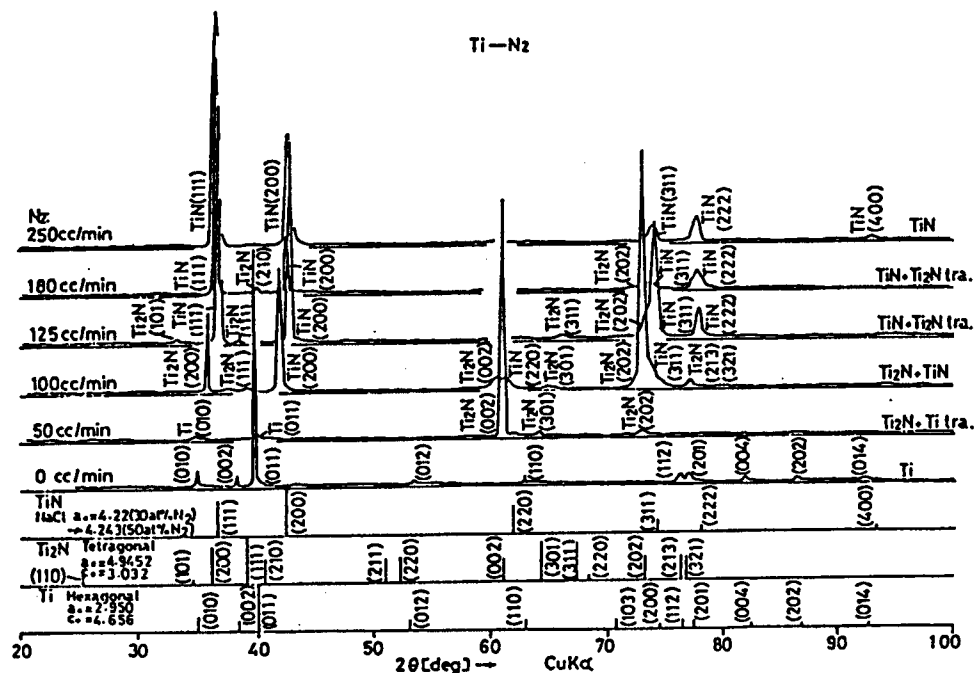


Figure 2. X-Ray Diffraction Intensity Exhibited by It-TiN Evaporated Film With Nongradient Composition

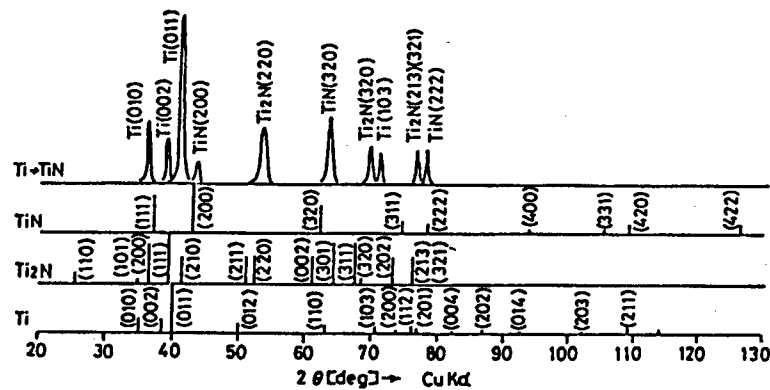


Figure 3. X-Ray Diffraction Intensity Exhibited by It-TiN Evaporated Film With Gradient Composition

Figure 4 shows the results of analysis of the gradient composition It-TiN film conducted using an EPMA and the Knoop hardness values recorded at the corresponding points of the same sample. It is seen from Figure 4 that even though the nitrogen gas flow rate was linearly increased, the film composition changed in stages. To manufacture an It-TiN composite whose composition is graded as designed, it is important to appropriately control the nitrogen gas flow rate. As for hardness, the TiN phase was the hardest, followed by the Ti_2N -TiN mixed phase, the It- Ti_2N mixed phase and the It phase in that order.

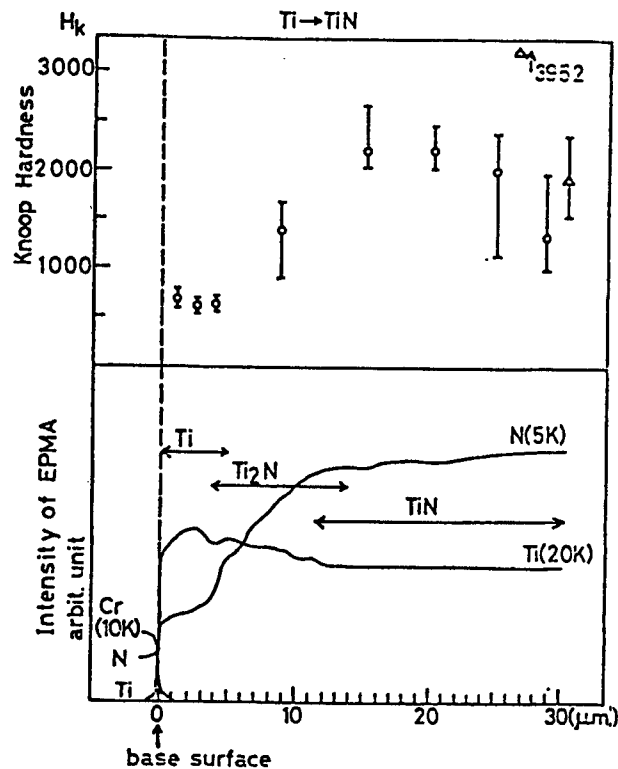


Figure 4. EPMA Intensity and Knoop Hardness of Ti-TiN Film With Gradient Composition

Figure 5 shows electron-micrographs of gradient composition Ti-TiN evaporated films and the corresponding diffraction patterns. The micrograph shown in Figure 5(a) is of a film portion close to the stainless steel substrate. The corresponding diffraction pattern indicates that this film portion consists of Ti. The micrograph shown in (b) is of a film portion at about half the film thickness. It is seen that this film portion contains TiN. According to the results of the abovementioned analysis conducted using an EPMA, this film portion was mainly comprised of Ti_2N , but the diffraction pattern indicates that it partially contained TiN, too. The micrograph shown in (c) is of a film portion near the film surface. The corresponding diffraction pattern indicates that this film portion consists of congregate fine TiN particles.

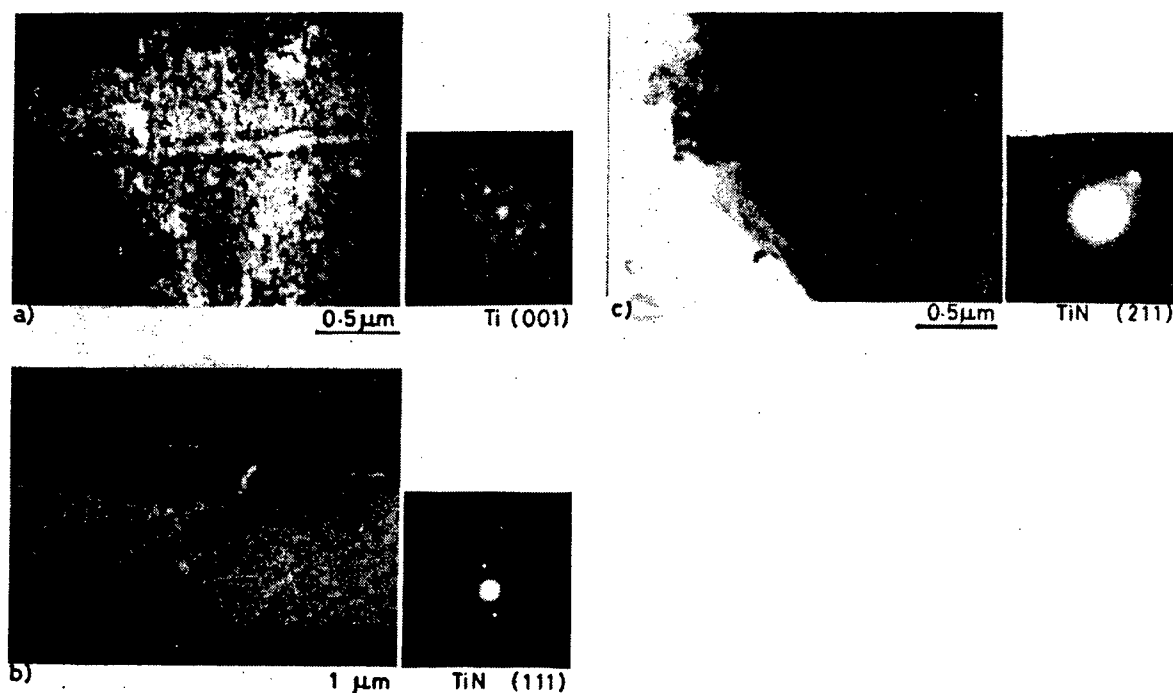


Figure 5. Electron-Micrographs and Diffraction Patterns of
Ti-TiN Film With Gradient Composition

4. Cr-CrN Evaporated Films With Nongradient Composition and With Gradient Composition

4.1 Cr-CrN Evaporated Films With Nongradient Composition

Cr-CrN films with nongradient composition were formed over stainless steel substrates by introducing a nitrogen gas at a constant flow rate into the vapor created by making chromium evaporate at a constant rate ($70 \mu\text{m/hr}$). Figure 6 shows the results of crystal structure analysis conducted using X-rays on film samples created in this way. As the nitrogen gas flow rate was increased, the composition of the evaporated film changed from a Cr phase to a Cr-Cr₂N mixed phase, then to a Cr₂N-CrN mixed phase and to a CrN phase. The CrN became free of Cr₂N only when the N₂ gas flow rate was raised to 200 cc/min. This is because chromium vaporizes faster than titanium.

4.2 Cr-CrN Evaporated Films With Gradient Composition

Cr-CrN films with gradient composition were formed over copper substrates by introducing a nitrogen gas at an increasing flow rate into the chromium vapor. The nitrogen gas flow rate was increased from 0 cc/min to 100 cc/min in 33 minutes at a constant rate of $10/3 \text{ cc/min/min}$. The reason for using copper substrates was to facilitate analysis of chromium and nitrogen using an EPMA.

Figure 7 shows the results of crystal structure analysis conducted using X-rays on film samples created in the above-described way. In Figure 7,

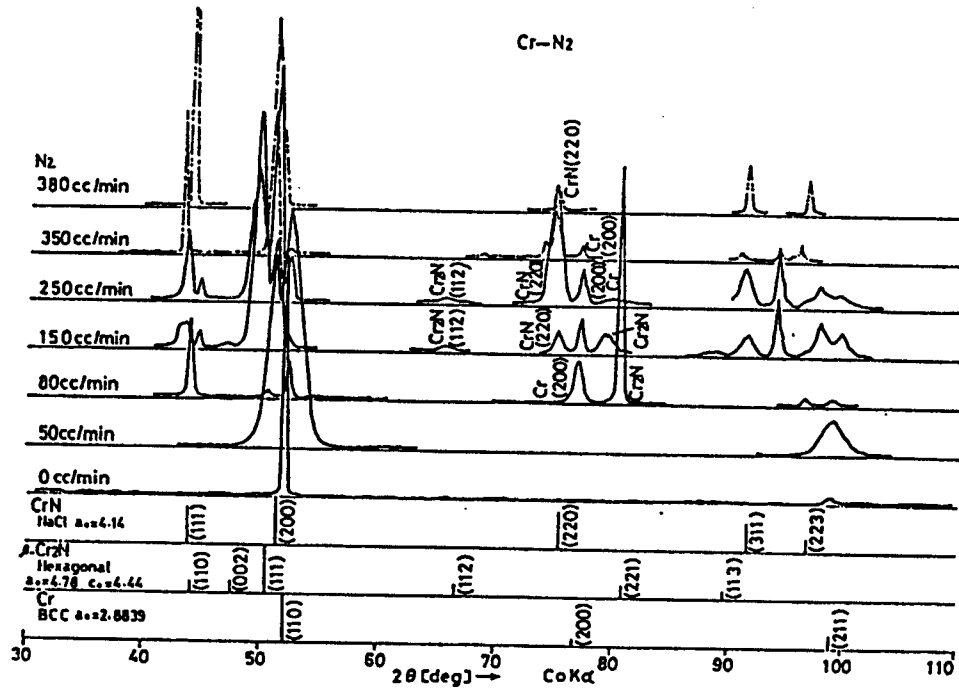


Figure 6. X-Ray Diffraction Intensity Exhibited by Cr-CrN Evaporated Film With Nongradient Composition

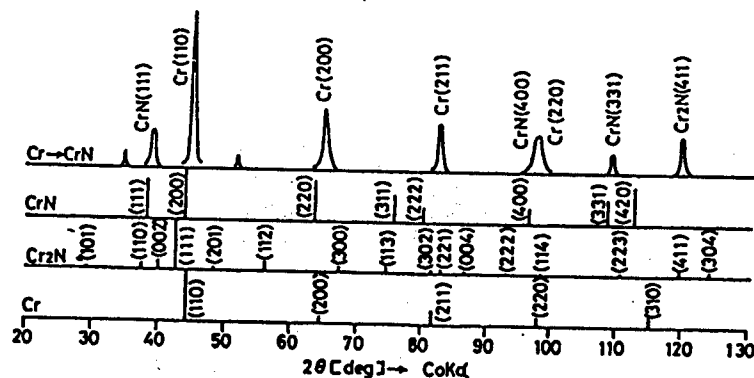


Figure 7. X-Ray Diffraction Intensity Exhibited by Cr-CrN Evaporated Film With Gradient Composition

strong diffraction lines from chromium and weak ones from Cr_2N and CrN are observed.

Figure 8 shows the results of elementary analysis conducted on cross-sections of Cr-CrN evaporated film using an EPMA and those of the corresponding Knoop hardness measurements. The results of the elementary analysis indicate that the concentration of N corresponds to that of the Cr- Cr_2N coexistent phase.

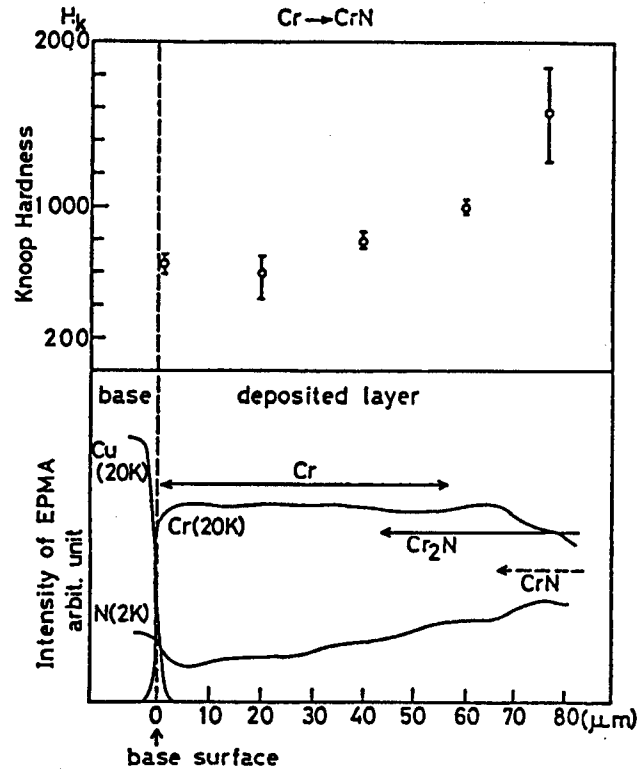


Figure 8. Results of EPMA Analysis and Knoop Hardness Measurements Conducted on Cr-CrN Evaporated Film With Gradient Composition

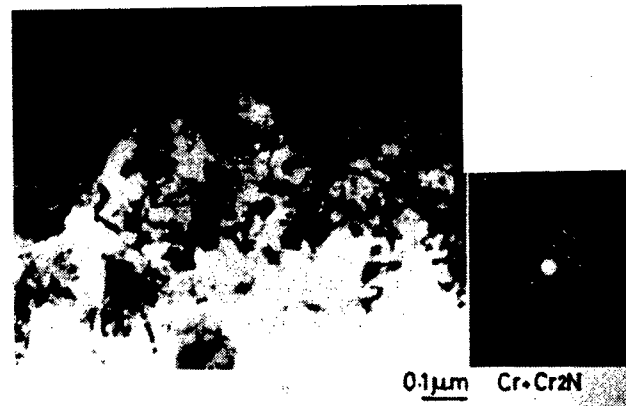


Figure 9. Electron-Micrograph of Section of Cr-CrN Evaporated Film With Gradient Composition and Corresponding Diffraction Pattern

Unlike in the Ti_2N evaporated film in which the composition was observed to change by steep steps, the composition change in the Cr-CrN evaporated film was gradual. It has been found that, because Cr vaporizes at a high rate,

the generation of a CrN phase requires the introduction of N at a higher density than necessary for the formation through evaporation of an It-TiN film with gradient composition. The Cr-CrN film exhibited high hardness due to the Cr₂N coexistent phase contained in it.

Figure 9 shows an electron-micrograph of a cross section of a Cr-CrN evaporated film with gradient composition and a corresponding diffraction pattern. It can be seen from Figure 9 that the film is made of congregate fine particles (1 μ m) of Cr₂N. The dislocation shown in the micrograph is assumed to have been generated when the sample was thinly cut out.

5. Conclusion

By means of the experiment we conducted, it has been found that It-TiN composites and Cr-CrN composites both with gradient composition can be created by the HCD type PVD process. In this connection, it will be necessary in the future to establish a technique to achieve, through reaction-gas flow-rate control, the conditions for realizing designed composition changes in the evaporated film. In this paper, the results of our experiment in creating nitride films with gradient composition have been reported. We have also been experimenting in creating carbide and oxide films with gradient composition by the HCD-type PVD process. The results of these experiments will be reported at another time.

This research and development work was conducted as part of the "research on fundamental technology for the development of functionally gradient materials effective in thermal stress relaxation" financed by the Science and Technology Agency's fund for science and technology promotion and adjustment.

Green Sheet Manufacture From Ceramics-Metal Powder

43067606g Tokyo KEISHA KINO ZAIRYO KENKYUKAI in Japanese 1 Jul 88 pp 25-30

[Article by Akihide Yoshitake, et al., Ultimate Materials Research Room, No 2 Materials Research Department, Nippon Kokan K.K.'s Steel Laboratory: "Study on the Manufacture of Green Sheet From Ceramics-Metal Powder"]

[Text] 1. Introduction

The R&D project "research on fundamental technology for the development of functionally gradient materials effective in thermal stress relaxation" financed by the Science and Technology Agency's fund for science and technology promotion and adjustment was inaugurated in FY 1987. This R&D project is aimed at developing new functional materials with properties controlled continuously and intentionally along the direction of their thickness to obtain the function of relaxing the thermal stress generated under severe operating conditions.

This R&D project with the above-stated goal supports the development of ultrahigh-heat resistant materials indispensable in the development of next-generation aircraft and spacecraft. And considering that materials developed under this R&D project will also be used in such fields as nuclear power, electronics, and medicine, it is an R&D project of some significance.¹

NKK [Nippon Kokan K.K.] took part in the material development project as a manufacturer (in connection with material structure control) and carried out basic research on the method of material manufacture. As a result, we proposed a green sheet lamination process as a method of material structure control. In this process, green sheet is made from slurry prepared, using doctor blades,^{2,3} from ceramics-metal powder of various mixing ratios, and the green sheet is then laminated and sintered into functionally gradient materials.

This process has the following features: 1) the green sheet thickness can be controlled in the range of several μm to about 2 mm; 2) this process is more suitable for mass production than other methods of green sheet manufacture; 3) the green sheet manufactured by this process is high in plasticity and moldability so that it can be used to manufacture parts in complicated shapes; and 4) the green sheet manufactured by this process can be used with relative ease as material for large structural members. In

FY 1987, our research was carried out on the following points with the main aim of acquiring fundamental data on the manufacture of green sheet:

- (1) Establishment of the technique for slurring ceramics-metal powder
- (2) Evaluation of green sheet
- (3) Observation of the structures of sintered bodies including laminations

An outline of our research conducted on the above points follows:

2. Green Sheet Manufacture From Powder

The process to manufacture green sheet from powder is broadly divided into the following subprocesses:

- (1) Mixing process during which the starting powder and additives such as binders are mixed and the powder is uniformly dispersed
- (2) Defoaming process during which the slurry is defoamed and its viscosity is adjusted
- (3) Green sheet manufacture by the use of doctor blades
- (4) Green sheet drying
- (5) Green sheet lamination
- (6) Green sheet degreasing and sintering

These processes are illustrated in Figure 1.

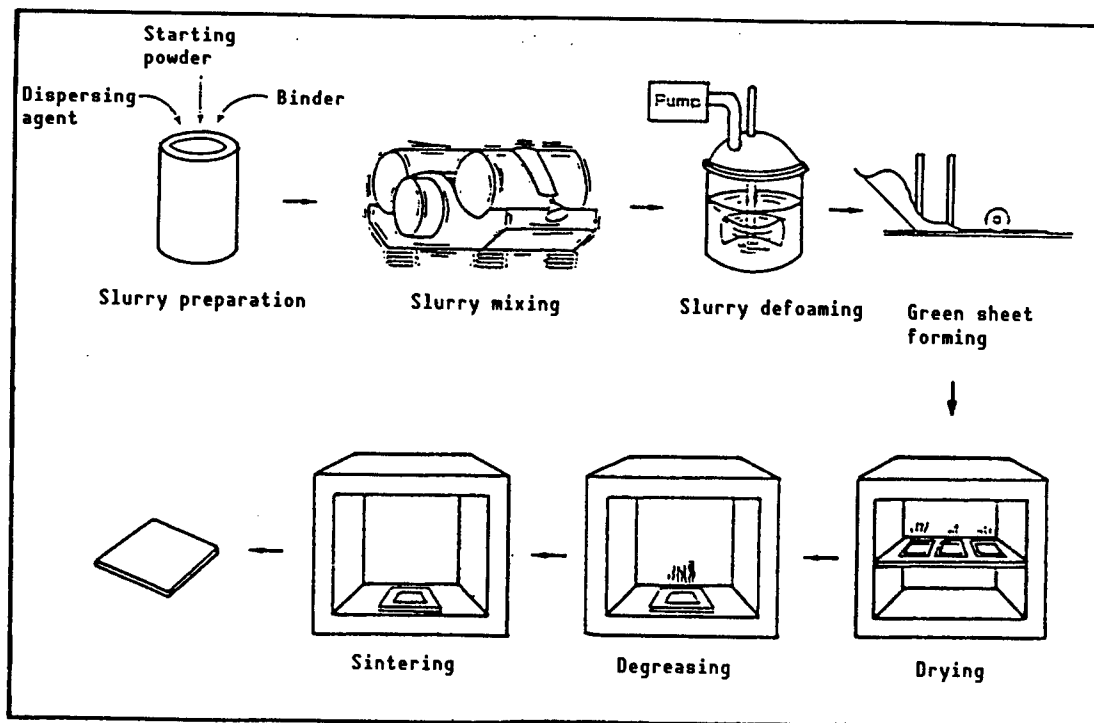


Figure 1. Process To Create Green Sheet From Powder

3. Green Sheet Manufacture

In our research, we used Al_2O_3 powder (measuring $0.4\ \mu\text{m}$ in average particle diameter) and ZrO_2 (measuring $0.03\ \mu\text{m}$ in average particle diameter) as ceramic materials and Ni powder (measuring $4\ \mu\text{m}$ in average particle diameter) as a metallic material. These materials were mixed with such additives as an acrylic binder, a dispersing agent, and a plasticizer using a vibration mill. The mixing time should be dependent on the state of particle dispersion in the slurry. In reality, however, it is difficult to ascertain the state of particle dispersion in the slurry. Therefore, we conducted grading analysis on the particles contained in a dilution of the slurry and determined the mixing time based on the results of the grading analysis. Figure 2 shows the relationship between the slurry mixing time and the average particle diameter. As seen from Figure 2, the average particle diameter stays almost unchanged after the mixing time reaches 5 hours. On this basis, we set the mixing time at 5 hours for our experiment.

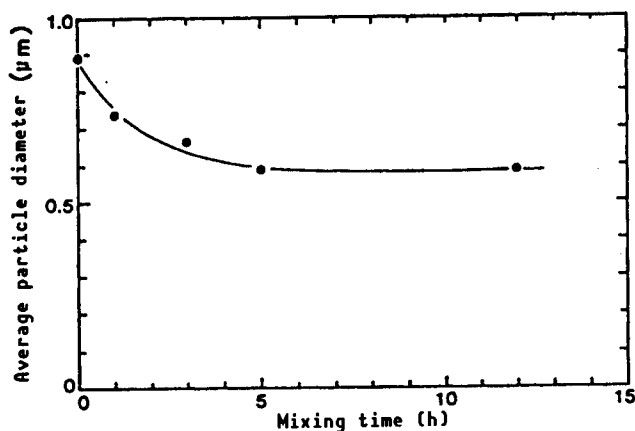


Figure 2. Relationship Between Slurry (Al_2O_3) Mixing Time and Average Particle Diameter

For slurry defoaming, a vacuum agitating defoamer was used to reduce the time required and make viscosity measurement easier. At the same time as the slurry was defoamed, the solvent contained in it was recovered until its viscosity was 20,000-40,000 cps. The doctor blade thickness was set at 0.5 ~ 1.5 mm most of the time. Green sheets right after formation contain solvent at a high concentration. Rapid drying causes cracking. Figure 3 shows how the green sheet weight reduces with time during natural drying. Taking into account the data shown in Figure 3, we dried the green sheets in the air for about 24 hours after their formation, during which time their weight reduced noticeably. Subsequently, we dried them adequately using a thermostatic oven set at 50°C . They were then stored in a dry desiccator set at 22°C and 50 percent RH.

If the amount of binder used to manufacture green sheets is inadequate, the green sheets become cracked or cambered during the drying process. If the amount is too great, the green sheets remain adhesive even after they are

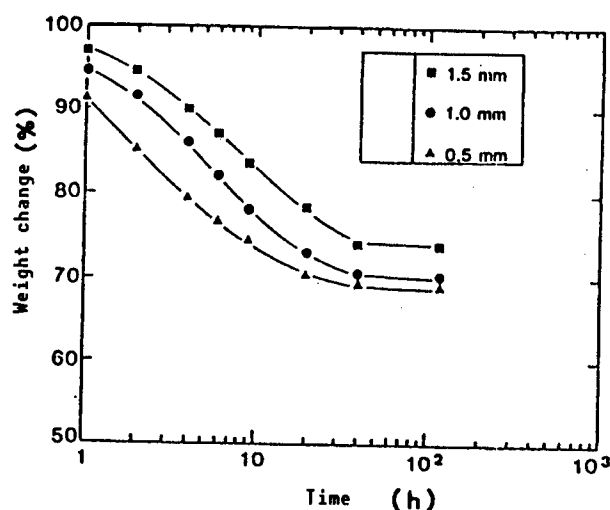


Figure 3. Changes in Green Sheet Weight During Drying (ZrO_2 at 20° and 50% RH) (Binder solid blending ratio: 28%)

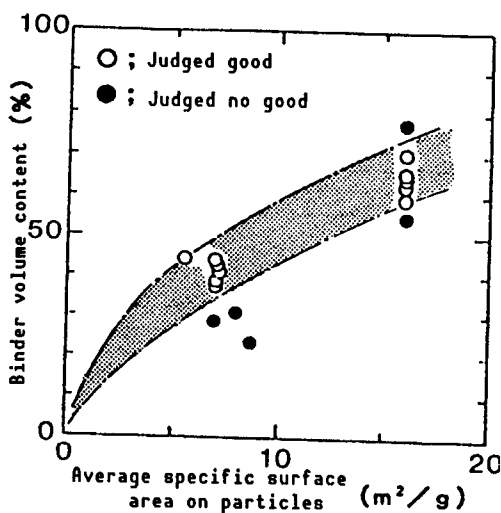


Figure 4. Appropriate Range of Binder Amount for Green Sheet Creation

dried, making them less easy to handle. The binder fills the space around and between the particles of the starting powder and binds them together. In Figure 4, the results of green sheet evaluation are shown in relation to the amount of binder and the specific particle surface area. It can be seen from Figure 4 that to manufacture quality green sheets, the amount of binder should fall within a certain range that can be determined based on the specific surface area of the starting powder particles.

4. Evaluation of Green Sheet Strength

The obtainability of complicated shape green sheet samples depends on the green sheet workability. We conducted tensile strength tests on green sheet samples to study the relationship between the tensile strength of green sheets and the amount of additives contained in them. The tests were conducted using a tension tester. As for the test pieces and test method, we complied with JIS K7113 (prescribing tensile tests on plastics).

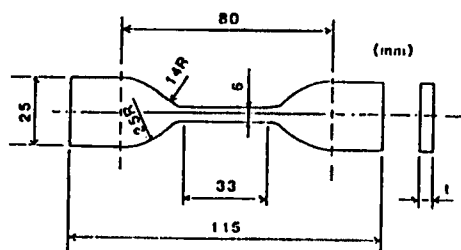


Figure 5. Test Piece Shape and Dimensions (mm)

Figure 5 shows the test piece shape and dimensions; Figure 6 shows samples of the test results. The green sheet strength and the Young's modulus tend

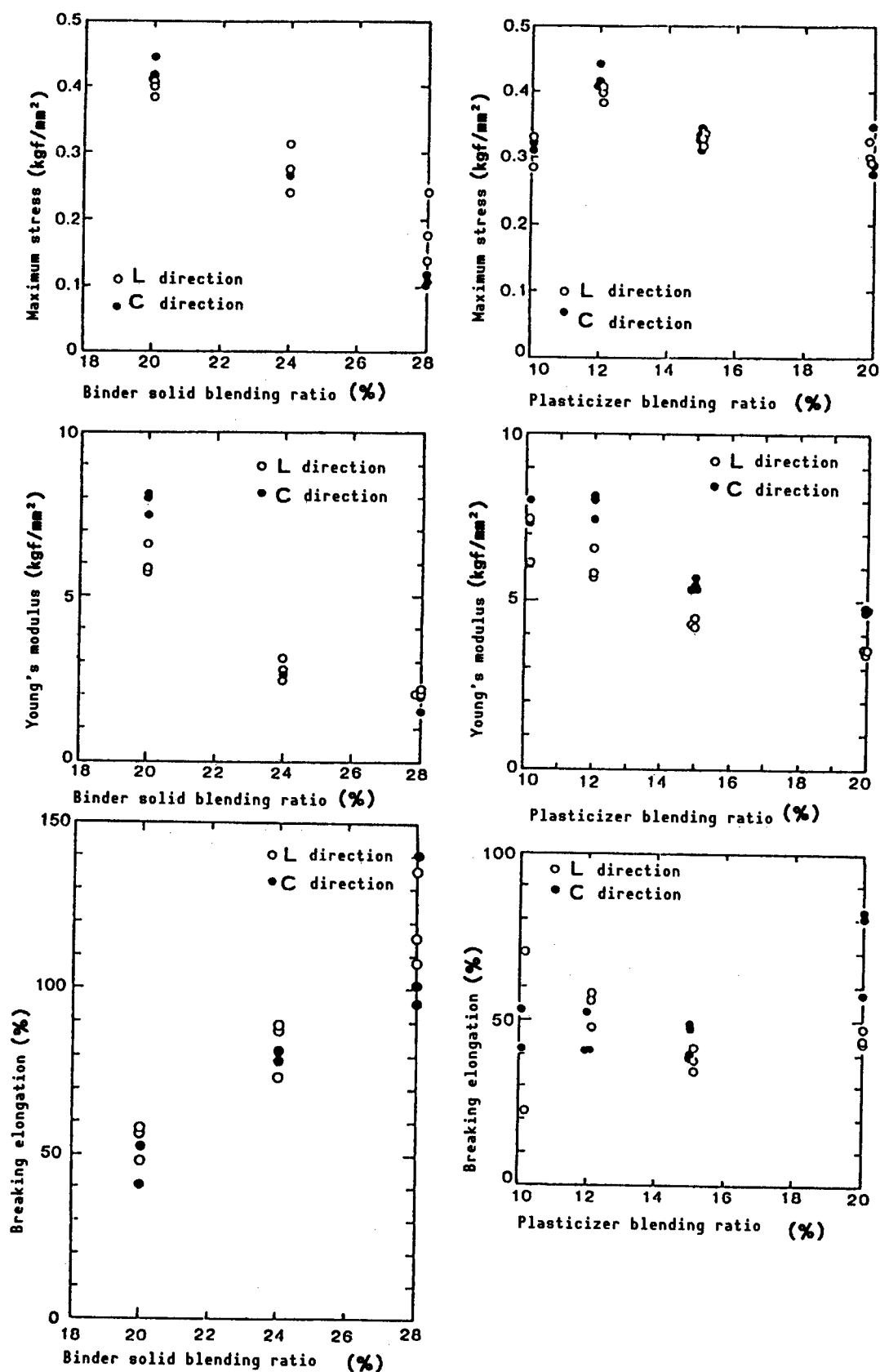


Figure 6. Dependence of Changes in Mechanical Properties of Al_2O_3 Green Sheet on Amounts of Binder and Plasticizer

to decline with the increase in the amount of binder they contain, whereas their breaking elongation increases with the binder amount. It has also been found that the Young's modulus, strength and breaking elongation of green sheet is not affected very much by the amount of plasticizers. Therefore, to manufacture green sheet samples in complicated shapes, it is desirable to determine the binder amount within an appropriate range depending on the degree of working complexity involved.

The green sheet samples we made and tested exhibited strength comparable to that of the conventional green sheet.⁴ It is considered to be superior in terms of quality, too.

5. Results of Observation of Green Sheet Sintered Bodies

For green sheet degreasing, we determined, after conducting thermal decomposition tests on the binder to be used, the maximum temperature (500°C) and the heating speed (10-30°C/hr) that are thought to result in complete binder decomposition without causing green sheet cracking. The results of our observation of the homogeneous material samples created by sintering green sheet at 1,350-1,550°C follow.

Photographs of the microstructures of ceramic samples are shown in Figures 7 and 8 [not reproduced] and those of samples comprised of ceramics mixed with 33 vol% and 67 vol% of metal, respectively, are shown in Figures 9 and 10 [not reproduced]. These photographs show that compared with the ceramics-only samples, those comprised of ceramics-metal mixtures contain considerably more residual pores around the half-thickness deep portion. It is also observed that, in the sample containing more metal than ceramics in terms of volume, the metal particles are bound in a manner to form a network and that, in the sample containing more ceramics than metal, the ceramic particles are bound as if forming a network. The structures of these samples resemble those of samples prepared by sintering powder by the dry method.^{5,6} The structure of a sample made of metal (nickel particles) only is shown in Figure 11 [not reproduced]. This sample can be seen to contain large pores, indicating that the pore ratio of samples sintered at the same temperature tends to rise in proportion to the metal particles contained in them. Figure 12 shows the relationship between the proportion of ceramic powder contained in green sheets and the pore ratio. It is thought that the samples we created by sintering green sheets had pores because no particular measure was taken to eliminate them. To reduce the pore ratio in sintered bodies, it is necessary to consider the adoption of an appropriate measure for pore removal for example, the utilization of HIP.

There are two methods that can be used to laminate green sheets. In one method, green sheets are laminated with a binding agent applied between them. In the other method, green sheets containing a binder are heated to soften the binder and they are then pressed for lamination. In our experiment, we adopted the second method, considering that the green sheets to be handled were on the μm order of thickness. Specifically, we pressed green sheets at about 10 MPa in atmosphere at 100°C. A photograph of a laminated sample (five-sheet lamination) we created is shown in Figure 13 [not reproduced]. With neither pores nor delamination observed at layer

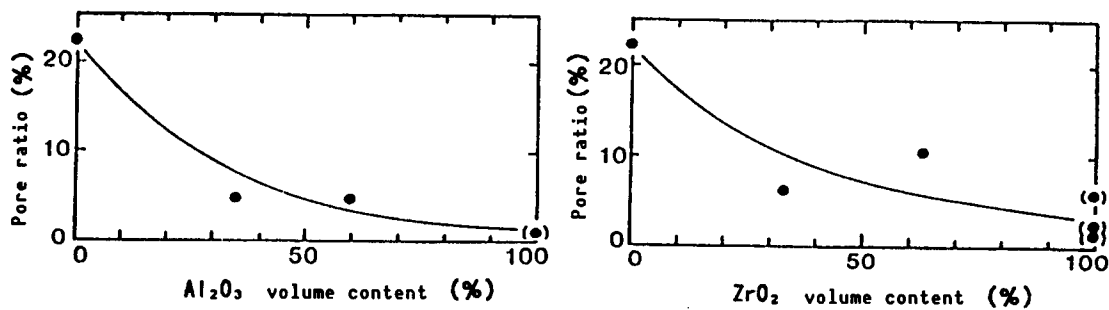


Figure 12. Relationship Between Ceramic Powder Content and Pore Ratio

boundaries in this sample, it is thought that we achieved quality lamination. We believe that the conditions under which this laminated sample was created are also applicable to the lamination of green sheets with various compositions.

8. Green Sheet Shrinkage Coefficient

Before creating a functionally gradient material by laminating green sheets with various compositions, it is necessary to ascertain adequately how much the green sheet dimensions change (coefficient of shrinkage) in the various processes involved. If a functionally gradient material is created without taking into account the green sheet shrinkage, it will camber or crack. Figure 14 shows the coefficients of shrinkage measured along the widths of various single-layer metallic green sheets during sintering. It can be seen from Figure 14 that the shrinkage coefficient varies with the metal particle mixing ratio. Specifically, it is observed that the coefficient of shrinkage tends to grow larger as the ratio of metal particles with small average diameters increases in the green sheet composition.⁷ Now, we intend to systematically study the effect of the ceramic powder mixing ratio in green sheets on their shrinkage coefficient.

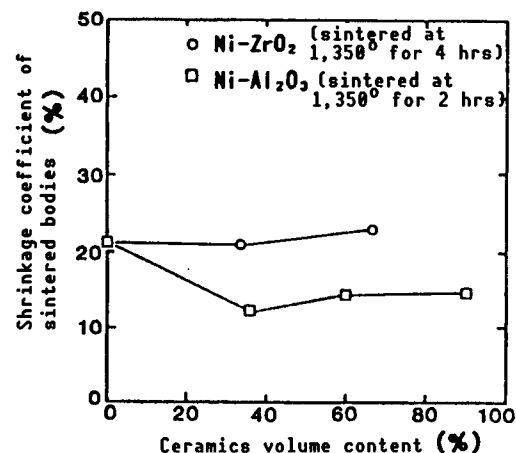


Figure 14. Shrinkage Coefficient of Ceramics-Metal Green Sheets (in width direction)

7. Conclusion

On the basis of the results of research on the manufacture of green sheets we carried out during FY 1987, we have presented an outline of the green sheet manufacturing process we proposed and the properties of green sheets created by this process. Due to space limitations, we have presented only a limited amount of data. Through our research conducted in FY 1987, the conditions to be met to manufacture green sheets of stable quality from a mixture of ceramics and metal powder have been made clear.

To realize the manufacture of functionally gradient materials using the process we proposed, it is essential 1) to study the optimization of the conditions for laminating green sheets with varied compositions, and 2) to systematically determine the coefficients of shrinkage during the sintering of green sheets with various compositions.

In FY 1988, we plan to fabricate a prototype pressurization-type green sheet sintering system that can be used to sinter green sheets while inhibiting cambering. While trying to determine more clearly the conditions to be met to laminate green sheets, we will aim at experimentally manufacturing functionally gradient materials.

References

1. M. Arano, "Design of Functionally Gradient Materials Using Complexation Technique," KINO ZAIRYO, Vol 7, No 10, 1987.
2. K. Murakawa, "Tape Molding," SERAMIKKUSU, No 3, 1977.
3. K. Saito, "Fine Ceramics Molding and Organic Materials," CMC.
4. K. Iwamura, et al., "High-Density Pore Elimination From Alumina Green Sheets," SOSEI TO KAKO (journal of Nippon Sosei Kako Gakkai [Institute of Plastic Working Engineers of Japan]), Vol 29, No 326, 1988.
5. "Report on a Survey of Fundamental Technology for Function Generation and Thermal Stress Relaxation Through Material Complexation," compiled under disbursement from the government fund for science and technology promotion and adjustment for FY 1987, May 1987.
6. M. Koizumi and Y. Tada, "Inauguration of Functionally Gradient Material Research Society and Its Role," KINZOKU, April 1987.
7. S. Munemiya and M. Yoshimura, "Zirconia Ceramics," Uchida Rokakuen.

Metal-Ceramics Film Formation by Separate Thermal Spray

43067606h Tokyo KEISHA KINO ZAIRYO KENKYUKAI in Japanese 1 Jul 88 pp 31-33

[Article by Take Fukushima, National Research Institute for Metals: "Metal-Ceramics Film Formation Through Separate Thermal Spraying"]

[Text] Introduction

The Structure Control Research Department of the National Research Institute for Metals has been taking part in the research project on the "fundamental technology for the development of functionally gradient materials effective in thermal stress relaxation" in connection with research on the technology for material structure control to be realized through lamination forming by the thermal spray method. Specifically, it has been assigned to research on the fundamental technology that enables the creation of functionally gradient materials through thermal spraying to be performed separately for different kinds of particles.

In particular, our task is to research the fundamental technology that can be used to form a film comprised of metal and ceramics mixed at a gradient ratio by separately thermal-spraying metal powder (mainly a nickel group alloy) and ceramic powder (mainly ZrO_2) using two plasma-spray torches in order to eventually establish the fundamental technology for the creation of functionally gradient materials capable of withstanding operating environments subjected to sharp temperature changes.

Contents of Research Conducted in FY 1987

During FY 1987, we experimented in forming laminations of metal (Ni-Cr alloy) and ceramic (ZrO_2 - Y_2O_3 8%) by thermal-spraying them separately, using a single spray torch, as a preliminary step before experimenting in forming laminations with gradient composition by the use of two plasma spray torches. In the experimental lamination forming, we varied such control conditions as the plasma operating current, the operating gas flow rate, the spraying distance, and the powder feed rate. The condition of thermal spraying performed and the laminations formed were studied in order to obtain information useful for determining the conditions to be met to form laminations with gradient composition.

Outline of Experiment Results

In this experiment, an Ni-Cr alloy and a $\text{ZrO}_2\text{-Y}_2\text{O}_3$ 8% ceramic were thermal sprayed using a plasma spray system, as shown in Figure 1, under the conditions listed in Table 1. We examined the condition of spray-material melting, the deposit efficiency and other factors observed during the experiment, analyzed the structures of films made from the two spray materials, and conducted tensile tests on samples of them.

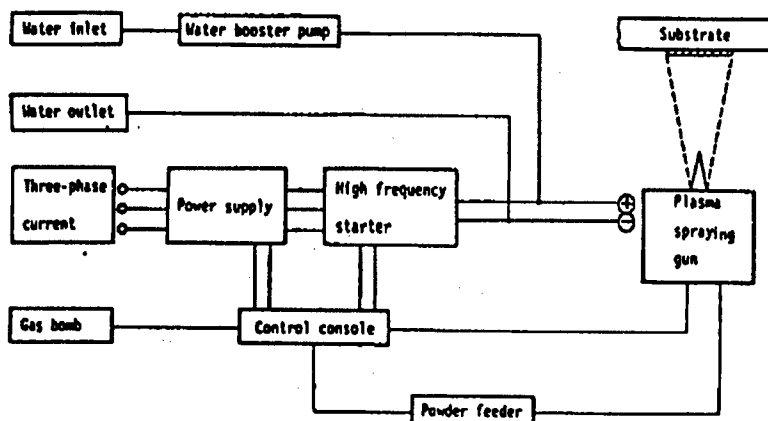


Figure 1. Plasma Spray System Structure

Table 1. Conditions of Experiment

	Thermal spray materials		
	Ni-Cr	$\text{ZrO}_2\text{-Y}_2\text{O}_3$ 8%	
Operating current: I (A)	600, 800, 1,000	1,000, 1,200, 1,400	
Flow rate of operating gas (Ar): G (ℓ/min)		30, 45, 60	
Powder feed rate: P (g/min)		5, 10, 20	
Particle size: (μm)		44 ~ 10	
Spraying distance: D (mm)	100, 150, 200		
Base metal	SUS 304 (3 t x 30w x 100 ℓ mm)		

(1) Conditions of Spray Material Melting

Varying thermal spray conditions did not result in any notable difference in the conditions of melting of the two thermal spray materials Ni-Cr and $\text{ZrO}_2\text{-Y}_2\text{O}_3$ that passed a plasma jet. Figure 2 shows the conditions of particles of the two thermal spray materials melted at various operating currents.

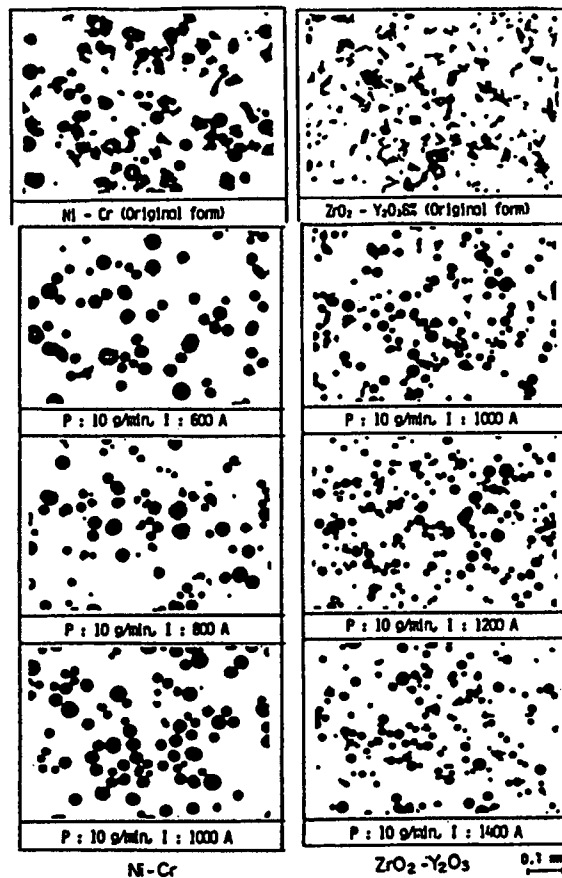


Figure 2. Conditions of Melted Particles

(2) Deposit Efficiency

For both the Ni-Cr alloy and the ZrO₂-Y₂O₃ ceramic, the deposit efficiency tended to rise with the increase of operating current and decline with the increase of spraying distance and powder feed rate. Figure 3 shows the results of deposit efficiency measurement performed under various conditions.

(3) Structure of Films Formed by Thermal Spraying

(a) Effect of Operating Current

The effect of the operating current on the structure of the Ni-Cr alloy film formed by thermal spraying is small. In the case of the ZrO₂-Y₂O₃ film, a larger operating current results in higher film quality with fewer pores. Figure 4 shows sectional views of the Ni-Cr and ZrO₂-Y₂O₃ film structures.

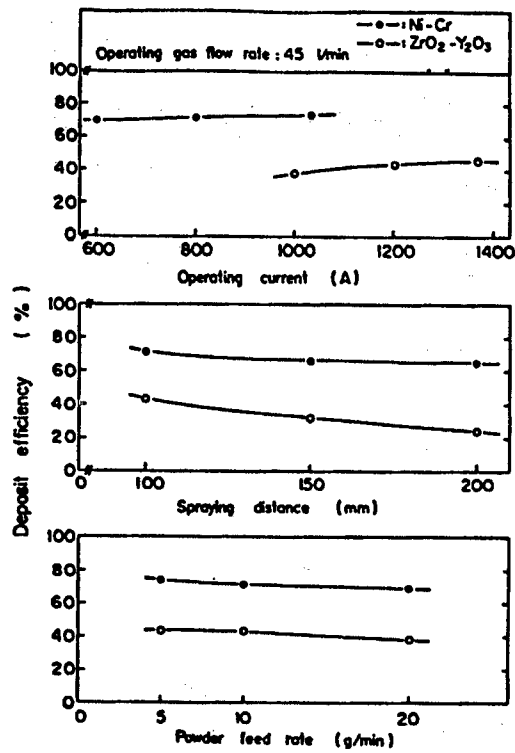


Figure 3. Deposit Efficiency

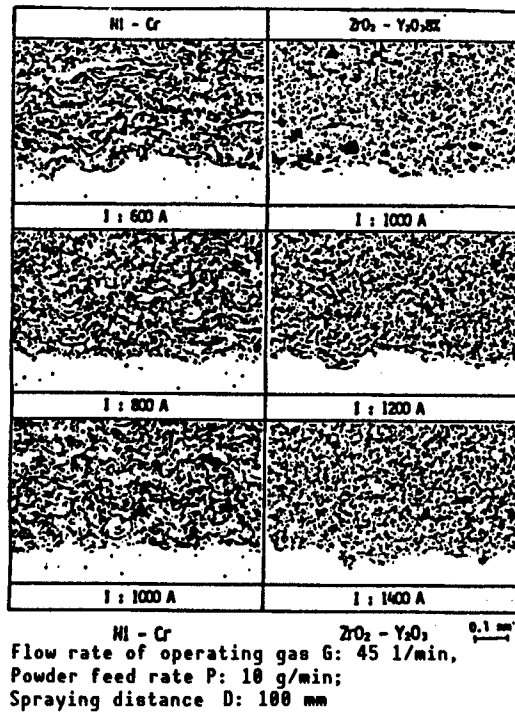


Figure 4. Structures of Films Formed by Thermal Spraying

(b) Effect of Operating Gas Flow Rate

The operating gas flow rate was observed to have no effect on the structure of the Ni-Cr alloy film, whereas it was found that a higher operating gas flow rate resulted in fewer pores in the $\text{ZrO}_2\text{-Y}_2\text{O}_3$ film.

(c) Effect of Spraying Distance

A longer spraying distance resulted in the generation of more oxides in the Ni-Cr alloy film and larger pores in the $\text{ZrO}_2\text{-Y}_2\text{O}_3$ film.

(d) Effect of Powder Feed Rate

No effect of the powder feed rate was observed on the structure of either the Ni-Cr alloy film or the $\text{ZrO}_2\text{-Y}_2\text{O}_3$.

(4) Tensile Strength of Films Formed by Thermal Spraying

As listed in Table 2, the Ni-Cr alloy film recorded a tensile strength of 19.8 MPa and the $\text{ZrO}_2\text{-Y}_2\text{O}_3$ film 8.4 MPa. Their tensile strength showed a tendency to increase with the increase in the operating gas feed rate.

Table 2. Tensile Strength of Films Formed by Thermal Spraying

	Thermal spray materials	
	Ni-Cr	$\text{ZrO}_2\text{-Y}_2\text{O}_3$ 8%
Operating current: I (A)	800	1,200
Flow rate of operating gas: G (ℓ/min)	45	45
Spraying distance: D (mm)	100	100
Tensile strength of sprayed coating (MPa)	19.8	8.4

Based on these results of our experiment, it has been found that the conditions for the thermal spraying of the Ni-Cr alloy can be controlled in a wide range without causing the resultant film structure to be significantly affected by the operating current, the operating gas flow rate or the powder feed rate and that a quality $\text{ZrO}_2\text{-Y}_2\text{O}_3$ film can be formed through thermal spraying at a high operating current and a high operating gas flow rate.

TiB₂-Cu FGM Synthesis by Self-Exothermic Reaction Method

43067606i Tokyo KEISHA KINO ZAIRYO KENKYUKAI in Japanese 1 Jul 88 pp 35-38

[Article by Nobuhiro Sada, Government Industrial Research Institute, Tohoku:
"Synthesis of Functionally Gradient TiB₂-Cu Composite Material by Self-Exothermic Reaction Method"]

[Text] 1. Introduction

The gradient function is a new concept related to the technique for joining or coating of different kinds of materials. When different materials are joined or when a material is coated with a different kind of material, the problem of thermal stress at the material interface occurs. Functionally gradient materials do not have interfaces between different kinds of materials (at least from the macroscopic viewpoint) and their gradient composition can be designed to relax thermal stress generation in them.¹ At present, a number of material synthesis methods are being researched with the aim of developing functionally gradient materials (FGMs) that are capable of thermal stress relaxation and can be used as heat-resistant materials. In this paper, the results of the experimental synthesis of an FGM comprised of TiB₂ and Cu we carried out by the self-exothermic method (SHS) will be introduced.

2. Theory and Features of Self-Exothermic Reaction Method

The self-exothermic reaction method is a material synthesis method that makes positive and efficient use of the reaction heat released at synthesis. It constitutes a new type of material manufacturing process totally different from the conventional material synthesis methods.² The theory of this self-exothermic reaction method is shown in Figure 1. In the self-exothermic reaction process, the synthesis reaction, started when the raw material is locally ignited, propagate spontaneously. Behind the raw material portion where the reaction occurs (reaction front), there is a high-temperature synthesis zone. In front of the reaction front, there is a preheating zone. The preheating zone is constantly provided with heat from the high-temperature synthesis zone behind the reaction front, and the heat is used to induce and maintain new reactions. In this way, the synthesis of a compound progresses while the induction energy needed for synthesis is supplied through the self-reaction of the raw material. Thus, this process, unlike conventional compound synthesis processes, does not

require that the raw material be heated externally, for example, by being kept in a hot furnace for extended periods. Furthermore, when this method is used, the synthesis reaction progresses second by second and the compound synthesis is completed at a very high temperature, resulting in a high synthesis ratio. Therefore, it may be said that this synthesis process is an energy-and cost-saving compound synthesis method. The compounds that can be synthesized by the self-exothermic reaction method are said to total some 100 or even 200 kinds, including--in addition to oxides--nitrides, carbides, borides, silicides, and sulfides. Recently, research on the techniques for simultaneously synthesizing and press-forming ceramics has been making headway. It is expected that these techniques being researched will be greatly improved in the field of composite material development from now on.^{3,4,5,6}

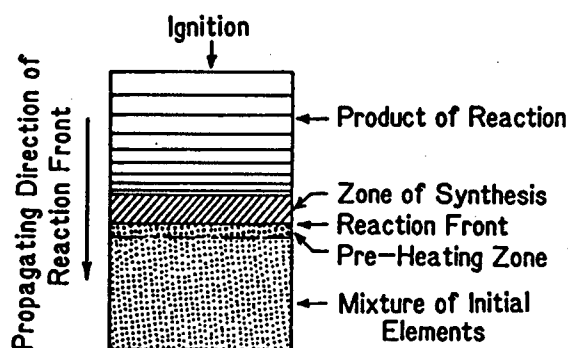


Figure 1. Schematic Diagram of SHS-Process

3. Technique for Simultaneous Synthesis and Forming

The self-exothermic reaction method makes it possible to mold a compound through sintering simultaneously as it is synthesized from a raw material. The sintering is carried out utilizing the high reaction heat generated during the reaction process.

Various techniques for realizing simultaneous synthesis and forming have been proposed.^{3,4,5,6} Most compounds, excluding oxides and nitrides whose coefficients of shrinkage cannot be easily calculated, undergo a volume shrinkage of 20 ~ 30 percent with respect to the corresponding raw material volume when they are synthesized by the self-exothermic reaction method.⁶ When the space between their particles is taken into account, their shrinkage coefficient must be considered close to 50 percent. The self-exothermic reaction progresses very rapidly, second by second. Therefore, to mold a compound as it is synthesized, a pressure effective enough to follow its shrinkage must be applied to it at the instant it undergoes reaction. In the case of such compounds as borides and carbides with high melting points, their melting points are only barely reached by the temperature of the system of reaction. Therefore, to mold these compounds, it is necessary to make provision for applying pressure to them in an appropriate way. Figure 2 illustrates the two methods of compression molding used by the author, et al.¹ In the spring pressing method

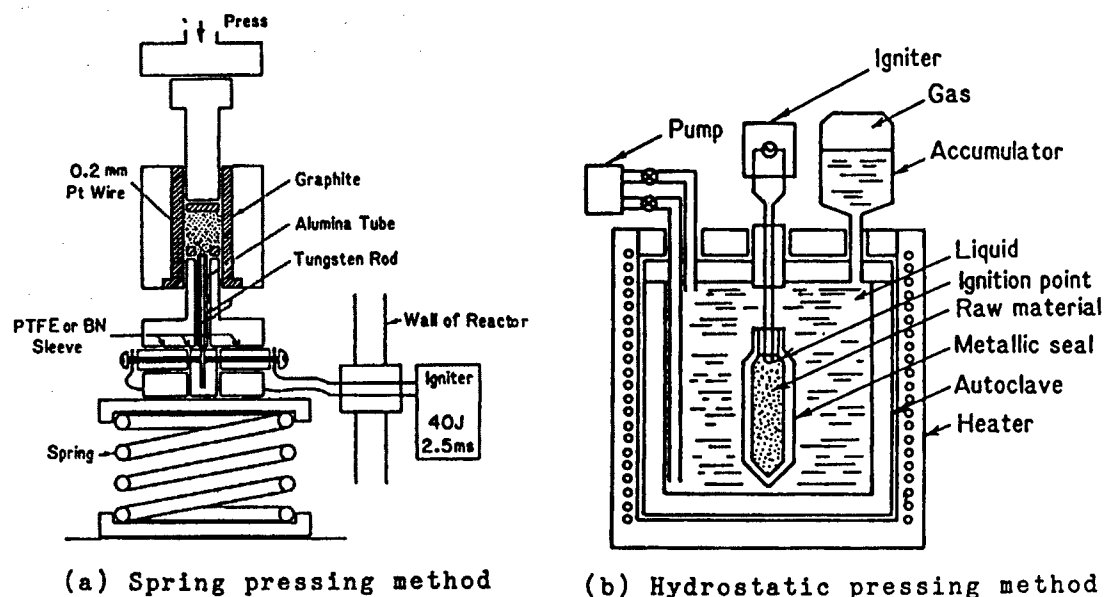


Figure 2. Experimental Apparatus for Simultaneous Ceramic Synthesis and Forming Under a Self-Propagating Reaction

illustrated in Figure 2(a), the pressing is uniaxial. In the hydrostatic pressing method illustrated in (b), the pressure is applied isotropically. In the uniaxial pressing method, the direction of the reaction propagation coincides with that of pressurization. It can therefore be said to be an efficient pressing method. However, while this uniaxial pressing method is effective in making small cylindrical samples, it is difficult to use in synthesizing materials in plates or other complicated shapes. Therefore, gas pressurization or the hydrostatic pressing method, as shown in Figure 2, will be more advantageous for commercial purposes. The hydrostatic pressing method is about 10 times more economical than the gas pressing method. In addition, this method is relatively easy to use. Considering these factors, it is expected that the utilization of this method as an economical technique for simultaneous ceramic synthesis and forming will be promoted in the future. At the Government Industrial Research Institute, Tohoku, we have been experimenting in synthesizing samples using the spring pressing method and have been evaluating their thermal and mechanical properties with the eventual aim of developing a technique for wide-range control of the ceramic synthesis to be carried out by the hydrostatic pressing method.⁷

4. Suitability of $\text{TiB}_2\text{-Cu}$ as Material for Functionally Gradient Material Synthesis

The requirements to be met in FGM synthesis by the self-exothermic reaction method include the following:

- (1) In the case of metal-ceramic composites, the surface layer must be comprised of a ceramic only.

(2) The FGM composition must be gradient in such a way that metal phases start appearing at a certain depth and that the metal content then gradually increases, resulting in a metal-only innermost region. The temperatures of the regions containing metal phases in the FGM must be kept, as the minimum requirement, below the melting point of the metal when the FGM is put in use.

(3) To use the self-exothermic reaction method for synthesis, the condition under which the synthesis reaction can be propagated must be arranged. The composition of an FGM must be continuous even in a region near a metal-only phase. Basically, a material with such a composition cannot be synthesized by the self-exothermic reaction method. However, synthesis is enabled if the heat generated in the synthesis reaction taking place on the ceramics-rich side of the raw material is conveyed to the metal-rich side.

For the present study, we have selected TiB_2 -Cu as the material to be synthesized into an FGM by the self-exothermic reaction method. The reasons for our selecting TiB_2 -Cu include the fact that Cu or Cu alloys are already in use as materials for structural parts of rockets and that the synthesis of TiB_2 involves great heat generation, making additive control easier and enabling thermal and mechanical property control over a wide range. For these reasons, TiB_2 -Cu appears to be an optimum material for use in fundamental research on FGMs.

5. Gradient Composition Control for TiB_2 -Cu

As the raw materials, It powder (-350 mesh), Cu powder (-325 mesh), and amorphous B powder ($-0.5 \mu\text{m}$) are used. In addition, TiB_2 powder ($3-5 \mu\text{m}$) is used for temperature adjustment. The raw materials used to synthesize a sample total about 2 g in weight. For sample synthesis, the spring pressing method is used. The pressure is applied over a sectional area of 100 mm^2 . After the raw material powder is filled in, it is preliminarily pressed at 50 MPa. It is then synthesized in a vacuum at 25 MPa into a formed sample measuring about 5 mm in thickness. Since no powder laminating system is yet available for our use, we synthesize FGM samples of multilayered structures. We made TiB_2 -Cu composite samples comprised of 2 to 21 layered units of different mixing ratios and conducted X-ray line analysis on them using an EPMA to determine the minimum number of units required to make the composite equivalent to an FGM. As a result, smooth composition curves were obtained from the samples comprised of 11 or more units. A microphotograph of a 16-unit sample is shown in Figure 3 [not reproduced]. The X-ray intensity curves obtained from It, B, and Cu contained in the same sample are shown in Figure 4.

With reference to the microphotograph, the leftmost layer consists of TiB_2 only, and the rightmost layer is comprised of Cu only. Two layers containing many pores can be observed, one in the center and the other near the Cu-only layer. It is assumed that in the central layer with a relatively low Cu content, heat tended to be contained during the synthesis process, causing the boiling point of Cu to be exceeded and eventually preventing the layer from being structured with adequate tightness. As for

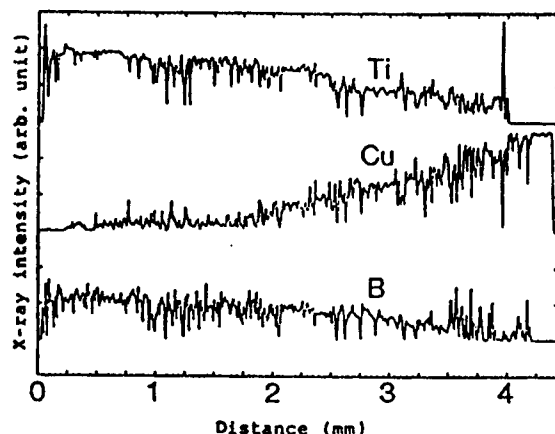
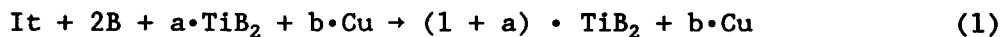


Figure 4. X-Ray Line Analysis of Ti, Cu, and B on the White Line in Figure 3

the other layer with many pores observed near the Cu-only layer, it is assumed that the amount of heat with which the layer was provided was not enough to tighten the layer structure. The X-ray analysis intensity curves shown contain large vibrations. This is due to the fact that the TiB_2 -Cu composite has a dual phase structure comprising a Cu matrix in which TiB_2 particles are dispersed.

Using the following equation (1), we calculated the maximum temperature (T_{max}) reached by the system of reaction during intermittent reaction occurrences. As a result, it has been found that the compound structure or its pore ratio can be controlled by adjusting the amounts of TiB_2 and Cu to be used.



6. Conclusion

Not many years have passed since research for the development of materials by the self-exothermic reaction method was started, so the accumulation of relevant data is still small. In these circumstances, the development of functionally gradient materials--which cannot be achieved without a high level of reliable technology--constitutes a great research object. We think that there is still a long way to go before the objective can be accomplished. However, research in this direction has another aspect that is quite attractive, and that is the development of a technique for thick-layer coating or for providing materials with additional functions. In this respect, at least, it can be said that the direction of research being promoted is not wide of the mark, even though there are many related research subjects yet to be tackled--for example, the feasibility of combining the self-exothermic reaction method and the CVD method or the necessity of postprocessing, both as a means of obtaining functionally gradient materials with acid resistance.

The contents of our research on the manufacture of functionally gradient TiB_2 -Cu composites by the self-exothermic reaction method have been briefly discussed. At the next symposium, data on the thermal and mechanical properties of materials with nongradient composition that we collected to obtain information useful in developing a system for layered powder filling or in designing functionally gradient materials will also be introduced.

References

1. Sata, KINO ZAIRYO, Vol 8, No 2, 1988, pp 47-58.
2. Ikeuchi, Odawara, and Sata, SANSHAIN JANARU [SUNSHINE JOURNAL], Vol 6, No 4, 1985, pp 24-28.
3. Odawara and Ikeuchi, NIPPON KINZOKU GAKKAISHI, Vol 45, 1981, pp 316-321.
4. Y. Miyamoto, M. Koizumi, and O. Yamada, JOURNAL OF AMERICAN CERAMICS SOCIETY, Vol 67, 1985, pp C224-225.
5. Sata, Report of Government Industrial Research Institute, Tohoku, Vol 19, 1986, pp 33-38.
6. Sata and Ikeuchi, YOGYO KYOKAISI, Vol 95, 1987, pp 243-247.
7. Sata, FGM NYUSU, No 1, May 1988, p 19.
8. N. Sata, K. Nagata, N. Sanada, T. Hirano, and M. Niino, MRS International Meeting on Advanced Materials, Tokyo, Japan, June 1988.

Research on Si_3N_4 -MO Ceramic With Gradient Composition

43067606j Tokyo KEISHA KINO ZAIRYO KENKYUKAI in Japanese 1 Jul 88 pp 39-42

[Article by Nobuhisa Tsutsumi, Casting Laboratory of Waseda University:
"Fundamental Research on Si_3N_4 -Mo Ceramic With Gradient Composition"]

[Text] 1. Need for Ceramics With Gradient Composition

Recently, research on the joining of metals and ceramics has been actively promoted with the aim of developing techniques applicable to the manufacture of ultrahigh-heat-resistant materials. The molten metal joining with ceramic that the author, et al., have been researching has in many cases resulted in cracks in the ceramic portion near the joint interface, mainly due to the stress generated when the molten metal solidifies and contracts. It appears that there are still many problems to be solved concerning the relaxation of thermal stress, in particular, before molten metal joining with ceramics can be established as a practical process. If metal-ceramic composites with controlled gradient composition can be manufactured, joining metals and ceramics will no longer be difficult. Among the techniques that can possibly be used to achieve controlled gradient compositions of metal-ceramic composites are the PVD, CVD, and particle arrangement methods. In the particle arrangement method, two kinds of powders with widely different properties are mixed and molded into gradient composition compacts that are subsequently hardened by sintering. Manufacturing this type of composite material requires both kinds of powders to undergo tightening in approximately the same temperature range. Since the sintering temperature for ceramic powder is generally higher than that for metal powder, it is necessary either to develop ceramic powder that can be sintered at a low temperature or else a new unique sintering technique.

2. Structures of Gradient Composition Ceramics

Unlike a joint between two metals, in a metal-ceramic joint large steps in the modulus of elasticity, the thermal expansion coefficient, the thermal conductivity and ductility are formed. In particular, when the molten metal solidifies and contracts after being joined with ceramic, stress is generated at the joint, causing the joint or ceramic portions near the joint to crack. In such zones of the joined material, cracks are highly propagative, so that even microscopic cracks are likely to develop into major cracks. As a means of preventing this, attempts are being made to

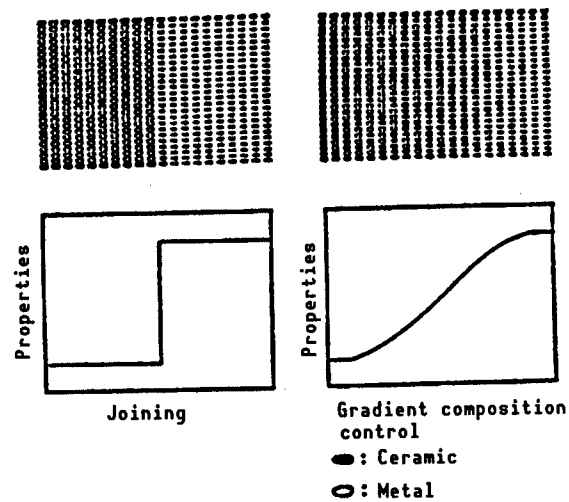


Figure 1. Schematic Diagram of Gradient Composition Control

design materials comprised of metal and ceramic mixed at gradient ratios that can be molded into structural parts. The type of composition required of these materials is schematically shown in Figure 1. It is a gradient composition with one end consisting of 100 percent ceramics and the other end 100 percent metal and with the intermediate portion between them composed of both ceramic and metal mixed at a gradient ratio. When a metal-ceramic composite material has this type of composition, it is possible, unlike in the case of metal-metal composites, that the properties of its intermediate composite portions may turn out to be inappropriate, in terms of strength or in some other respect, for the material to be used in structural parts. Therefore, depending on the case, it may become necessary to add other elements to the composition, so the number of ingredients of the composite material may not be limited to two (Figure 2).

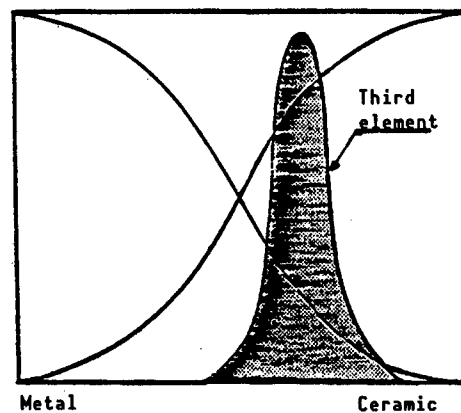


Figure 2. Ingredient Element Composition Distribution

In attempting to select the proper raw materials for a desired gradient composition composite material, design an optimum structure for it and develop a process to manufacture it, many problems are encountered that are associated with the conditions of environments for manufacture. Even when a process to manufacture the composite material is developed, the properties of the material manufactured using the developed process may turn out to be unable to meet the real application requirements. The problems that may be posed during these attempts should be solved by selecting or determining optimum conditions to be achieved at the level of each of the five stages or factors involved, i.e., raw material selection, material design, manufacturing process, evaluation, and composite material.

This paper reports on the results of the fundamental experiments conducted (by Tsutsumi and Yoshida) with stress on the analysis of problems with the process to manufacture a metal-ceramic composite material with gradient composition. The experiments were carried out without regard to the prospects of availability of gradient functions.

3. Experiment Method and Results

For our fundamental research on the control of the gradient composition of a metal-ceramic composite material, we selected Mo powder as a metallic raw material with a high melting point, Si_3N_4 powder as a ceramic raw material, and Si as an additive to lower the sintering temperature with the aim of enabling nitriding bonding in a lower temperature range. Using these materials, we experimentally created an $\text{Si}_3\text{N}_4/\text{Mo}$ composite with controlled multilayered gradient composition by the particle arrangement method.

Figure 3 is a flowchart of this experiment. As shown, the Si powder and the Si_3N_4 powder were mixed at a weight mixing ratio of 6:4 (the mixture is referred to as 6-4SN in this paper). The 6-4SN was mixed with the Mo powder to prepare samples ranging in weight mixing ratio from 0 to 100 percent in 10-percent steps. A set of samples arranged to comprise a complete gradient composition were stacked to form a layered composite material and were compression-molded at 300 MPa so that each layer would be 1 mm thick after compression. The compressed composite compact with the controlled gradient composition was placed on a boat and the boat was put in a siliconit resistance furnace to sinter the compact in a nitride ambience for a certain time at a specific temperature.

Layer samples prepared to create gradient composition compacts, as mentioned above, were also compression-molded individually, each to a thickness of 3 mm. They were separately sintered and the changes in dimension and weight they underwent through sintering were recorded. Their behavior during sintering and the effects of sintering on their structures were also observed.

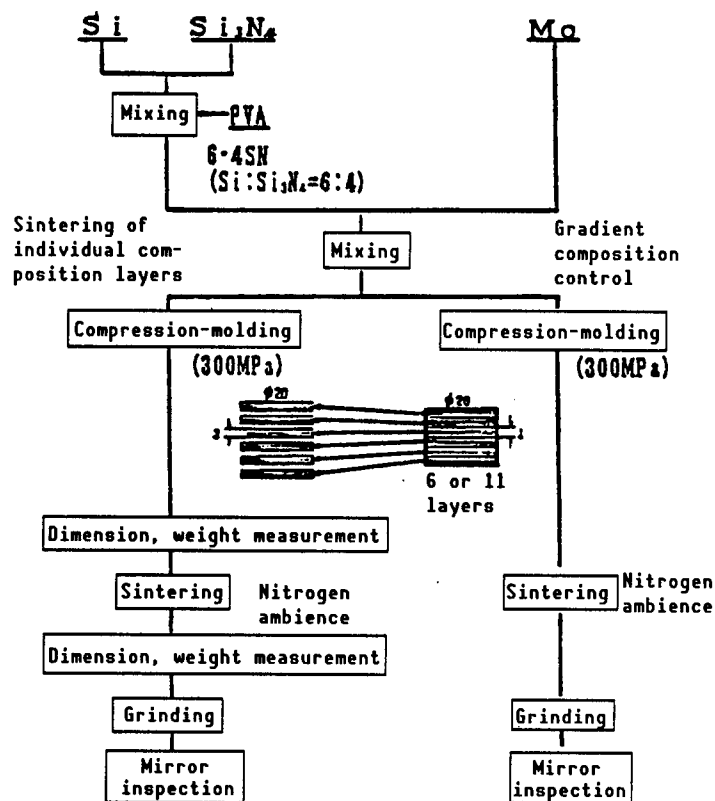


Figure 3. Flowchart of Experiment I.

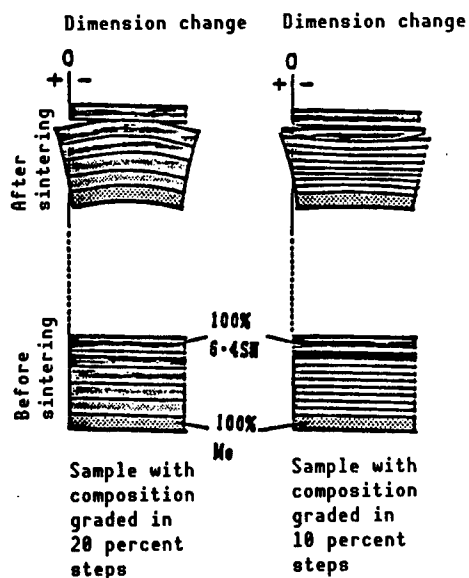


Figure 4. Conditions of Layered Composite Materials With Gradient Compositions After Sintering

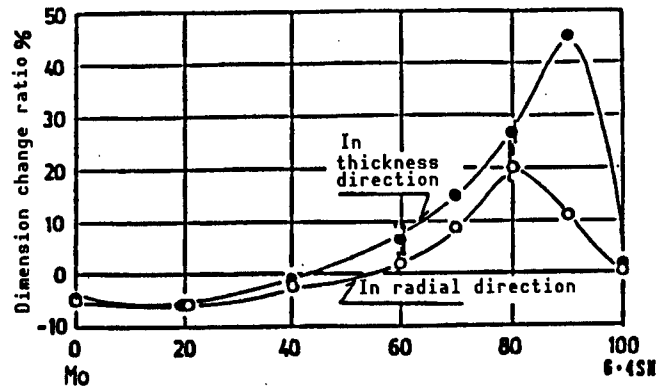


Figure 5. Effect of Raw Material Mixing Ratio on Dimension Change at Different Compositions (Samples sintered at 1,400°C for 10 hrs)

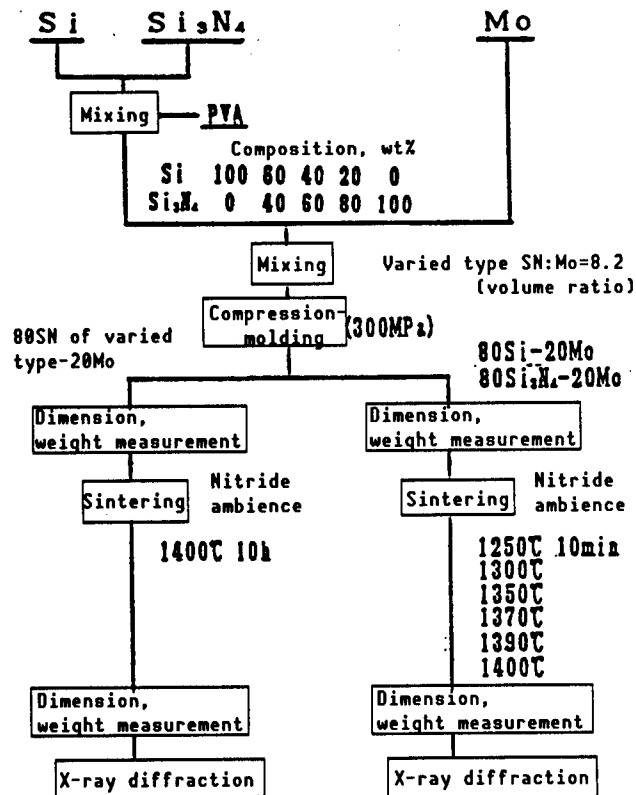


Figure 6. Flowchart of Experiment II

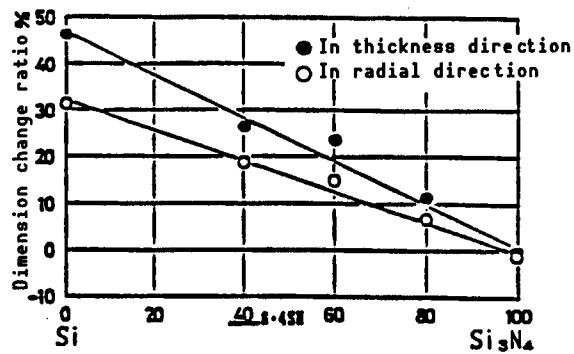


Figure 7. Effect of Raw Material Mixing Ratio on Dimension Change During Sintering (80SN of varied type-20Mo system, sintered at 1,400°C for 10 hrs)

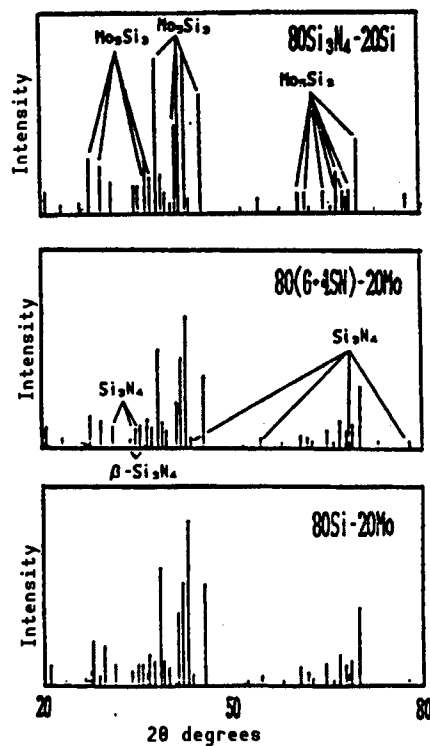


Figure 8. X-Ray Diffraction of 80 Varied Type of SN-20Mo System (Samples sintered at 1,400°C for 10 hrs)

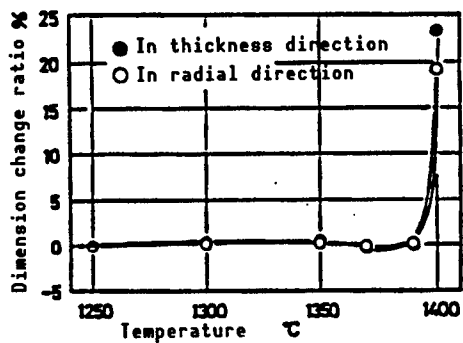


Figure 9. Sintering Behavior of 80Si₃N₄-20Mo System (Holding time: 10 min)

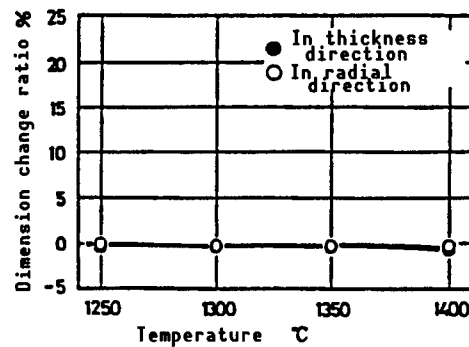


Figure 10. Sintering Behavior of 80Si-20Mo System (Holding time: 10 min)

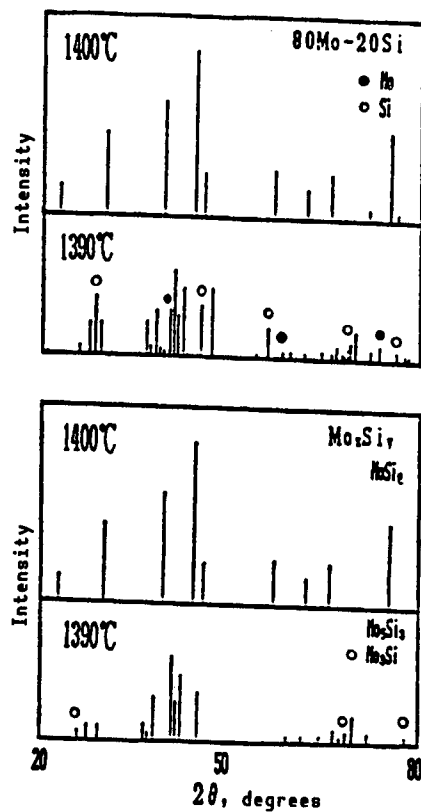


Figure 11. X-Ray Diffraction of 80Si-20Mo System Sintered at Various Temperatures

4. Problems and Tasks Associated With Development of a Process To Manufacture Metal-Ceramic Composite Materials With Controlled Gradient Compositions

- 1) Generation of intermediate portions of gradient composition composite material whose properties turn out to be improper for the intended application and development of a control method that can be used to eliminate this problem.
- 2) Selection of optimum ceramic materials for use in mechanical parts and the development of a process to manufacture composite compacts using the selected ceramics.
- 3) Development of a process to join the metal sides of composite materials having optimum gradient compositions with the corresponding metallic parts.
- 4) Utilization of a computer to design continuous gradient compositions of composite materials and establishment of a practical system for computer utilization.
- 5) Development of an optimum powder molding method that can be used to manufacture composite material parts in complicated shapes.

References

1. Tsutsumi and Furuta, Proceedings of 113th National Lecture Meeting of Japan Casting Association [Nippon Imono Kyokai], 1988, p 41.
2. Tsutsumi and Hatai, IMONO, 1988, not yet printed.
3. Tsutsumi, Hatai, and Furuta, Proceedings of the 113th National Lecture Meeting of Japan Casting Association, 1987, p 34.
4. Kagaku Gijutsu Koho Zaidan [Science and Technology Publicity Foundation], Report on Survey of Fundamental Technology for Material Complexation Effective in New Function Generation and Thermal Stress Relaxation.
5. Kawasaki, Murahashi, and Watanabe, Proceedings of Autumn Lecture Meeting of Nippon Kinzoku Gakkai [Institute of Metal Engineers of Japan], 1986, p 373.

Research on FGM Thermal Property Evaluation Technique

43067606k Tokyo KEISHA KINO ZAIRYO KENKYUKAI in Japanese 1 Jul 88 pp 43-46

[Article by Nobuyuki Araki, Faculty of Technology, Shizuoka University:
"Research on Functionally Gradient Material Evaluation Technique (Thermal
Property Evaluation Method)"]

[Text] 1. Introduction

In recent years, keeping pace with the progress in the fields of aeronautics and space, energy and electronics, many new advanced materials have been developed. When newly developed materials are to be used in parts to be subjected to high temperatures, the thermal property data (thermal conductivity, thermal diffusivity, specific heat, thermal expansion coefficient) on them are absolutely required. Therefore, collecting the thermal property data on new materials should be a prerequisite for promoting the development of advanced technologies. In reality, however, the accumulation of data on new materials is inadequate. The measurement of thermal properties involves various errors. To minimize the measurement errors, an optimum measurement method must be selected in accordance with, for example, the sample shape and dimensions, the measuring temperature range and the estimated magnitudes of thermal property values. Furthermore, adequate study must be conducted on measures to improve the measurement accuracy.

In the case of functionally gradient materials, because they are generally very thin, the scope of selection of measurement methods is extremely limited. Since their thermal properties are gradient within themselves, mere average property data on them are of no use. It is therefore necessary to establish a new evaluation method for them. It must also be noted that, when their thermal conductivity and diffusivity are measured, apparent values greater than the real ones are obtained. This is because the ceramic portions or pores contained in them transmit radiation.

We conducted theoretical and experimental studies in which the results can be used as the basis for selecting or developing thermal property measurement methods suitable for application to functionally gradient materials, and we also carried out experimental measurements on homogeneous samples by some selected measurement methods.

2. Measurement Methods and Measured Values

(1) Thermal Diffusivity Measurement by Step Heating Method

In the step heating method, the sample surface is heated by steps, the temperature responses are measured on the reverse side of the sample, and its thermal diffusivity is calculated based on the measurements. The system used for this measurement is schematically illustrated in Figure 1. Thermal diffusivity values measured on a sample relative to the standard sample MACOR are shown in Figure 2 (O represents a measurement obtained by the step heating method). It is seen that the measurements obtained in the 500 K to 700 K range are greater than the cataloged values. The sample was prepared by machining and had a diameter of 30.55 mm and a thickness of 3.245 mm.

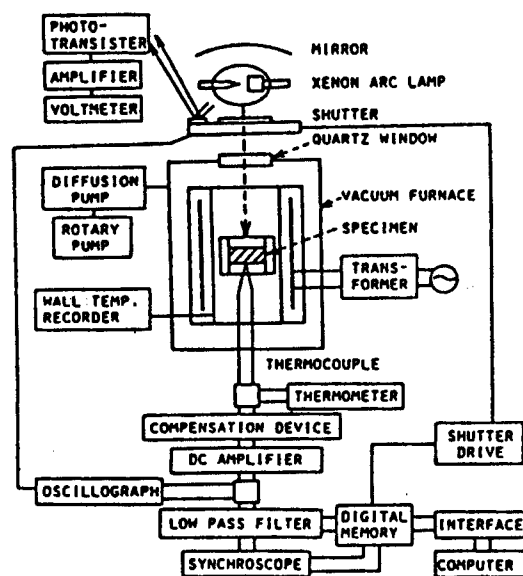


Figure 1. Step Heating System for Thermal Diffusivity Measurement

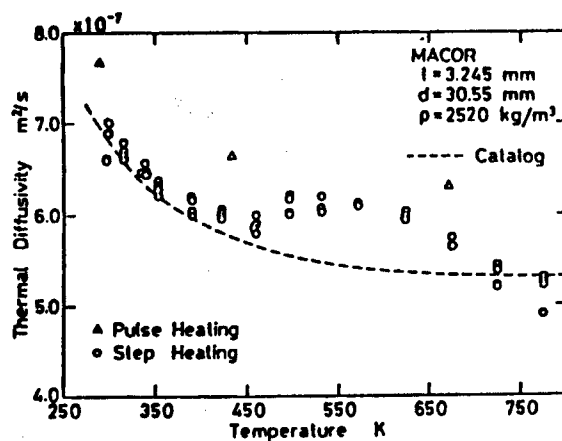


Figure 2. Sample Thermal Diffusivity Measurements

(2) Thermal Diffusivity Measurement by Pulse Heating Method

In the pulse heating method, the sample surface is heated using laser beam pulses, the temperature responses are measured on the reverse side, and the thermal diffusivity of the sample is calculated based on the measurements. Thermal diffusivity values measured on a sample relative to the standard sample MACOR are shown in Figure 2 (Δ represents a measurement obtained by the pulse heating method). The sample measured 10 mm in diameter and 0.525 mm in thickness. It can be seen that the values obtained by the pulse heating method are somewhat larger than those obtained by the step heating method. The reason for this has not been ascertained with the measuring system (TC-7000 made by Shinku Riko), which is not yet operable at full capacity. Figure 3 shows measurements taken on the sample PSZ (SUS 304-ZrO₂, ZrO₂ 60 vol%) prepared at the Watanabe Laboratory of Tohoku University.

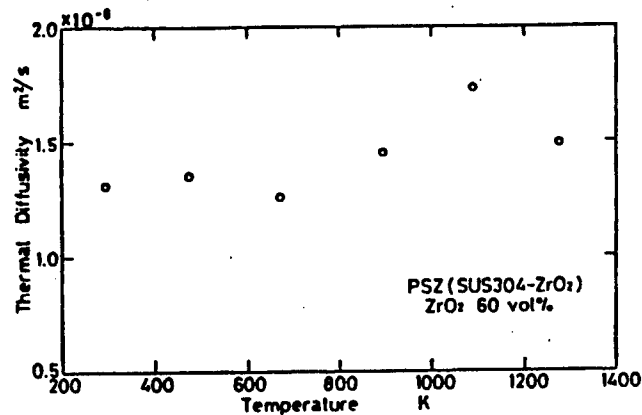


Figure 3. Thermal Diffusivity Measurements Taken on PSZ

(3) Specific Heat Measurement by ASC

Figure 4 shows specific heat measurements taken on a sample using an adiabatic scanning type calorimeter (SH3000MS made by Shinku Riko). As shown, the measurement curve rises slightly in proportion to the temperature. This measurement trend is not consistent with the cataloged data. The results of measurements performed using the ASC can be represented by the following equation:

$$C = 0.62 + 0.765 \times 10^{-3}T \text{ (KJ/Kg.K)}$$

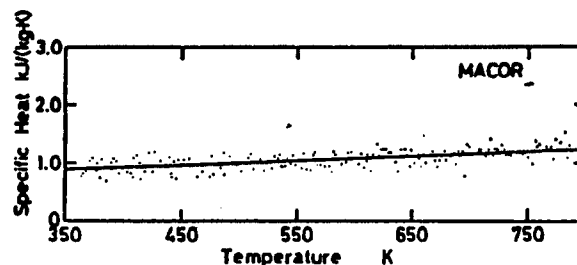


Figure 4. Specific Heat Measurements Taken Using ASC

(4) Thermal Conductivity

Values of thermal conductivity calculated based on the thermal diffusivity measurements taken by the step heating method and the catalogued values of specific heat and density are shown in Figure 5 (O). The corresponding values calculated based on the specific heat measurements taken using the ASC are also shown (O) in Figure 5. Other measurements listed in Figure 5 are thermal conductivity values calculated based on the thermal diffusivity and specific heat measurements taken by the pulse heating method (Δ), those directly measured by the steady-state method (\square) (C-MATIC made by Shinku Riko), and those obtained by the heat flow meter method at NAL [National Aerospace Laboratory] (\blacksquare).

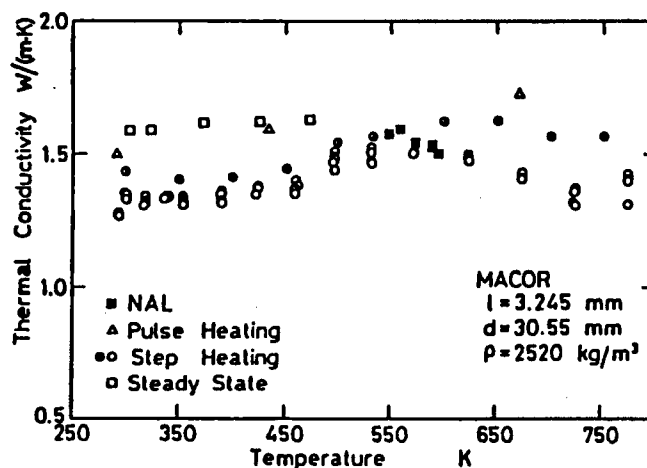


Figure 5. Results of Thermal Conductivity Measurements

(5) Coefficient of Thermal Expansion Measurement by Laser Beam Interference Method

Figure 6 shows the results of measuring the coefficient of thermal expansion of a standard sample MACOR using a dilatometer (LIX-1 made by Shinku Riko) designed to make measurement utilizing laser beam interference. As shown, the curve plotted through measurements at the rising temperature and that plotted through measurements at the lowering temperature did not coincide. The gap between the two curves can be narrowed by selecting a more appropriate rate of temperature rise.

3. Development of Thermal Diffusivity Measurement Method for Layered Samples and Establishment of Evaluation Method

We have developed a computation program to be used to determine the thermal diffusivity of three-layer samples using either the step heating method or pulse heating method. Figure 7 shows the relationship between Fourier number F_{02} and the heat capacity ratio of the second layer calculated on the basis of measurements taken by the pulse heating method. The curves plotted

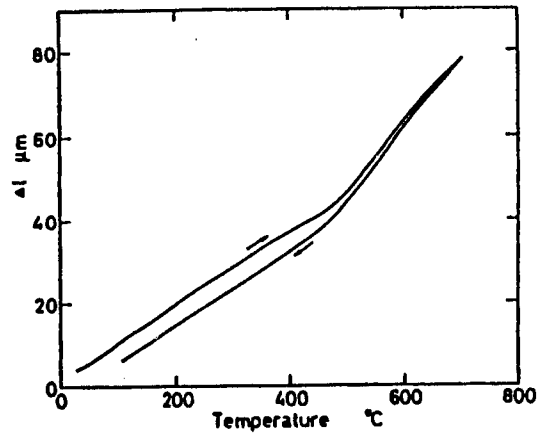


Figure 6. Results of Measuring Coefficient of Thermal Expansion

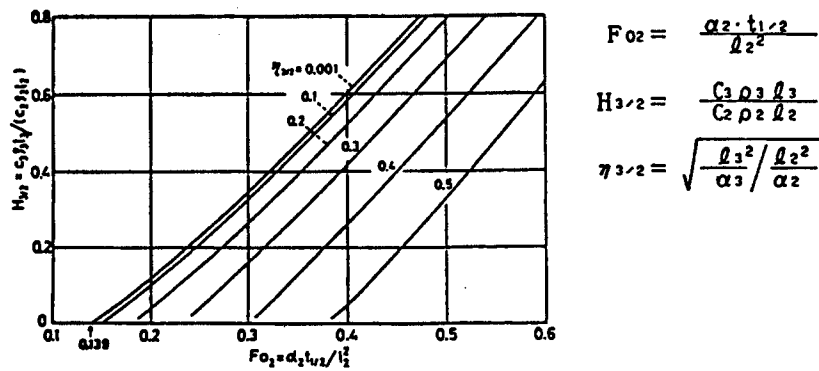


Figure 7. Relationship Between Fourier Number and Heat Capacity Ratio of Second Layer

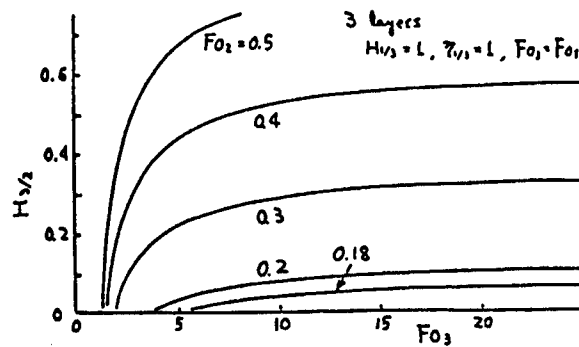


Figure 8. Fourier Numbers of Three Layers

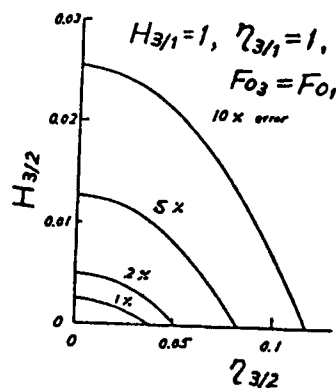


Figure 9. Coating Layer Errors

in Figure 7 represent examples of degrees of freedom of motion calculations made for the second layer of a three-layer sample, with the first and third layers consisting of the same material. Problems with the thermal diffusivity measurement that are dependent on the combination of property values of the sample have been analyzed (Figures 8 and 9). Figure 8 shows curves plotted to determine the thermal diffusivity of the first and third coating layers of a sample wherein the properties of the second layer are already known. It is seen that the value of F_{03} is difficult to determine where the value of F_{02} is small. If the first and third coating layers of a three-layer sample are ignored, errors as shown in Figure 9 result.

4. Future Research Policy

To further promote our research on the selection and development of processes to measure the thermal properties of functionally gradient materials, we will proceed next to research based on the following policies worked out for individual thermal properties:

(1) In connection with thermal diffusivity measurement, in addition to the step heating and pulse heating methods, other methods, for example, the periodical heating method, will also be studied. The goal of this study is to establish a method of applying selected measurement methods to thin-layered samples, a method of evaluating layered samples, and a method of estimating the radiation components of samples. Thermal diffusivity measuring experiments will be conducted not only on homogeneous samples but also on layered samples in a high temperature range (1,000 K or higher).

(2) As for specific heat measurement, the application of the ASC (adiabatic scanning calorimeter) method to solid samples at temperatures up to 1,000 K will be studied. An attempt will also be made to obtain higher measurement accuracy in the temperature range of ordinary temperature to 500 K by the use of a twin-type calorimeter.

(3) Regarding thermal conductivity, the development of a method of calculating the thermal conductivity of layered samples or functionally gradient samples based on the thermal diffusivity, specific heat and density values will be aimed at. Experiments in measuring thermal conductivity by

the steady-state method will be conducted using the high temperature fall fundamental evaluation system of NAL in order to probe the feasibility of thermal conductivity measurement at high temperatures.

(4) Regarding the coefficient of thermal expansion, measurement by the optical interference method will be studied and experimental measurements at high temperature (up to about 1,500 K) will be carried out.

Research on FGM Fracture Strength Evaluation

43067606h Tokyo KEISHA KINO ZAIRYO KENKYUKAI in Japanese 1 Jul 88 pp 47-50

[Article by Hideaki Takahashi, Material Strength Laboratory attached to Faculty of Technology of Tohoku University: "Functionally Gradient Material Evaluation Technique--Fracture Strength Evaluation Method"]

[Text] 1. Introduction

The project for the development of functionally gradient materials for thermal stress relaxation has entered its second year. As fruits for research conducted for the project, some materials have been experimentally developed and data on their properties have been reported. However, it is recognized that the standard testing methods applied to conventional materials do not suit functionally gradient materials. It is necessary to develop unique evaluation methods for application to functionally gradient materials.

Focusing attention on the activities of the property evaluation aspect among the three groups (design, synthesis, and evaluation) making up the core system for the abovementioned material development project, this paper will discuss the policies set out for the development of methods of material fracture tests and the progress of the joint research being carried out.

2. Role of Property Evaluation Group

The research subjects assigned to the property evaluation group are indicated in Figure 1. The research to be conducted on the evaluation of functionally gradient materials is divided into three subjects: 1) thermal stress evaluation; 2) heat insulation evaluation; and 3) fracture strength evaluation. Since these three research subjects are closely associated, the research institutes assigned to conduct research on them in the property evaluation group are required to promote research while maintaining close contact among themselves. Figure 2 shows an example of the evaluation sequence to be applied to samples developed by the synthesis group. As shown, evaluation data are to be reported to the synthesis or design group as they are produced.

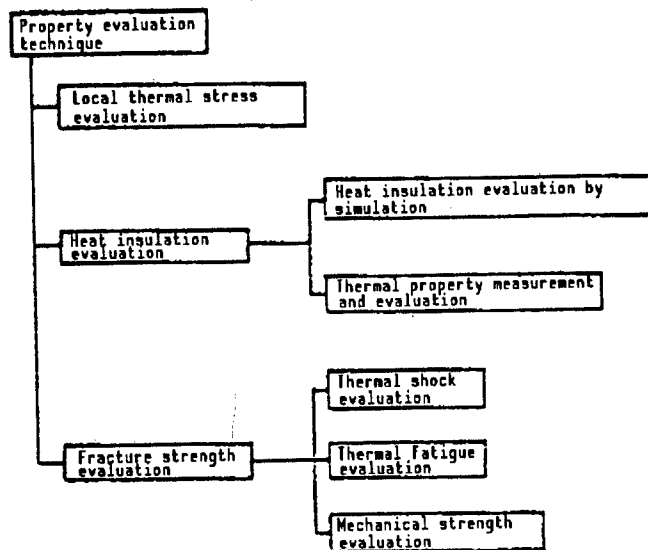


Figure 1. Classification of Property Evaluation

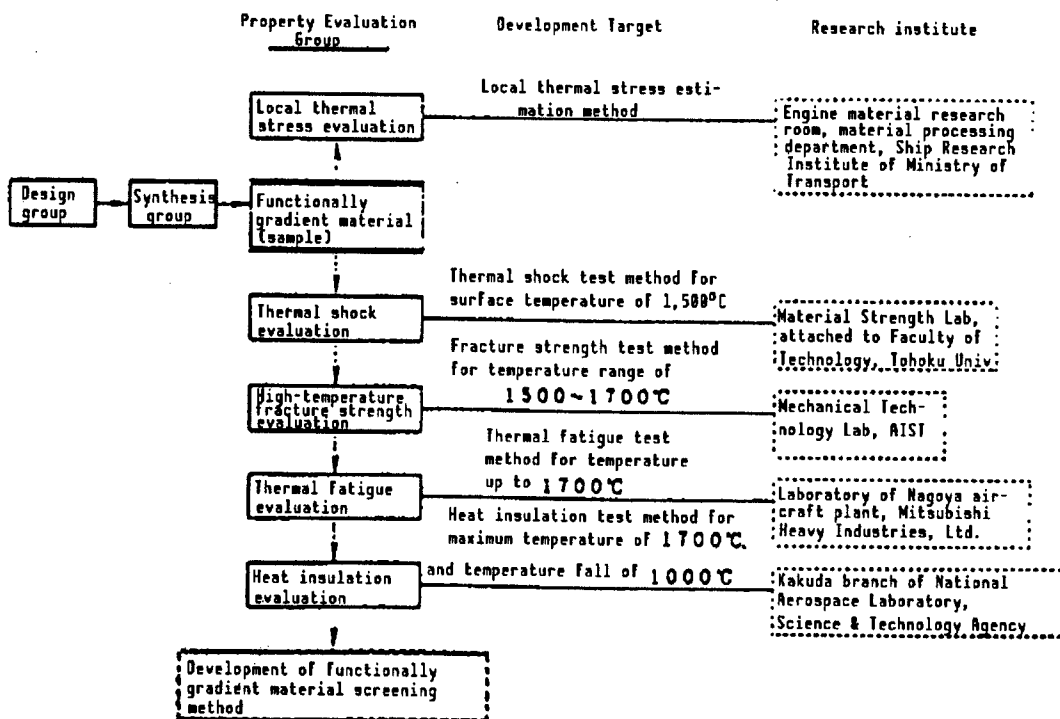


Figure 2. Property Evaluation Processes

3. Fracture Strength Evaluation Methods

The fracture strength evaluation methods being researched and related research items will be briefly discussed in this section.

(1) Small Punch Test Method^{1,2}

To computerize the designing of functionally gradient materials with priority given to the minimization of thermal stress generation, it is necessary to prepare a design database containing all kinds of premeasured material property data for every microstructure (base structure) that may be incorporated in functionally gradient material structures. The small punch test is a test method being developed as a standard method for use in collecting data to be entered in a material deformation and fracture database. In this test method, test pieces measuring $10 \times 10 \times 0.5 \text{ mm}^2$ are to be used. This is a convenient test method that enables accurate evaluation of the tensile fracture strength, yield strength, fracture strain, and Young's modulus of material samples.

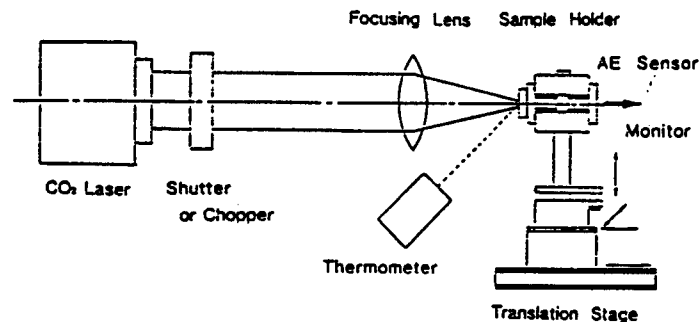


Figure 3. Use of Test Pieces for Small Punch Test

(2) Thermal Shock Test Method²

Experimentally produced functionally gradient materials are currently available in dimensions of 10-20 mm in diameter and 1-2 mm in thickness. Figure 4 schematically illustrates a thermal shock test system of the laser local heating type. This heating method is capable of both continuous and cyclic irradiation. In this test system, cracking caused by thermal stress in an unsteady state is nondestructively detected, enabling the damage due to thermal stress to be measured in a very short time.

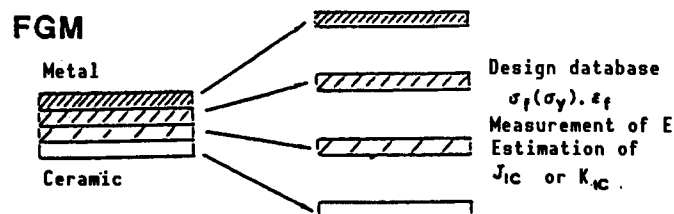


Figure 4. Schematic Diagram of Laser Heating Type Thermal Shock Test System

A working group to standardize thermal shock testing to be conducted by the use of a laser beam has been set up, and joint research has been started in the group using typical test materials.

(3) Thermal Fatigue Test

Thermal fatigue tests were formerly called repeated quench tests. A system used to conduct this test is schematically illustrated in Figure 5. The fundamental method of thermal fatigue testing is scheduled to be established through research to be carried out during FY 1987 and 1988.

(4) High-Temperature Bending Test and Fracture Toughness Test

The target temperature resistance set for functionally gradient materials to be developed is 2,000 K (about 1,700°C). Taking this into consideration, the development of methods of evaluating material strength at superhigh temperatures is aimed at. Typical evaluation methods being researched include the short rod sample evaluation method and the indentation method. A purpose of research on these evaluation methods is to find out fracture mechanics parameters associated with the deformation or fracture behavior of functionally gradient materials.

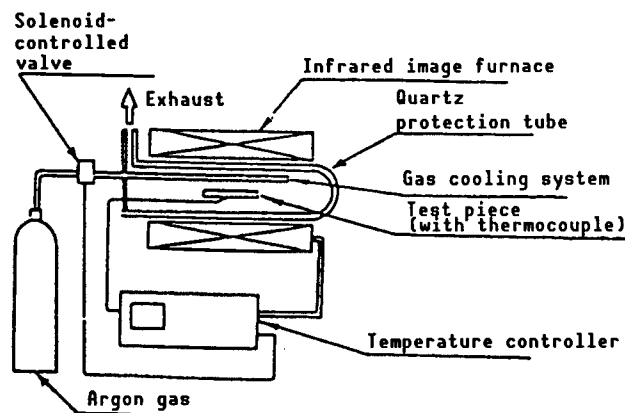


Figure 5. Schematic Diagram of Thermal Fatigue Test System

(5) Heat Insulation Evaluation Test by Simulation

The purpose of this heat insulation evaluation test differs from that of fracture strength evaluation. Since it is essential to evaluate the fracture strength of the surface as well as inner portions of functionally gradient materials exposed to increasing thermal stress, heat insulation evaluation methods and test system have been jointly researched in the material property evaluation group. Figure 6 shows the high temperature fall fundamental evaluation system introduced at the Kakuda branch of the National Aerospace Laboratory in FY 1987. The steady-state thermal stress applied in this test system is estimated at 5 MW/m². At the National

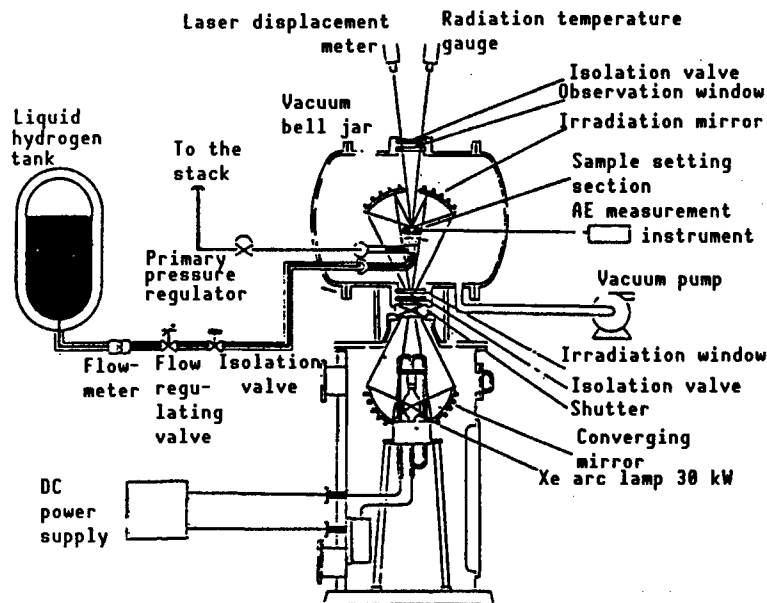


Figure 6. High Temperature Fall Fundamental Evaluation Test System

Aerospace Laboratory, the preparation for introducing an aerodynamic superheating field evaluation system capable of simulating Mach 6 is also underway.

4. Structuring of Functionally Gradient Material Databases and Standardization of Material Property Evaluation Method

If research being conducted for the functionally gradient material development project progresses as scheduled and various databases are prepared as planned, the flow of design, synthesis, and evaluation data in the system organized to promote the project should be as shown in Figure 7. With regard to the preparation and use of data on functionally gradient materials, it is most important to create various databases and knowledge databases. In this regard, it is essential that the data to be entered in the databases be collected through testing performed by the standard test methods determined on the basis of a consensus of all the groups making up the system organi to promote this project, as shown in Figure 7. In this sense, a most urgent task to be tackled now for this project is test method standardization. Therefore, provisional standard test methods should be worked out as soon as possible.

Figure 8 schematically illustrates, with attention focused on databases, the relationships between this functionally gradient material development project and the space shuttle development project that involves the development of an actual airframe and an engine in which functionally gradient materials are to be used. Figure 8 also suggests that while functionally gradient materials to be developed for the present project are small in dimensions, the design criteria to be set in the future for the space shuttle project should be taken into consideration in developing and

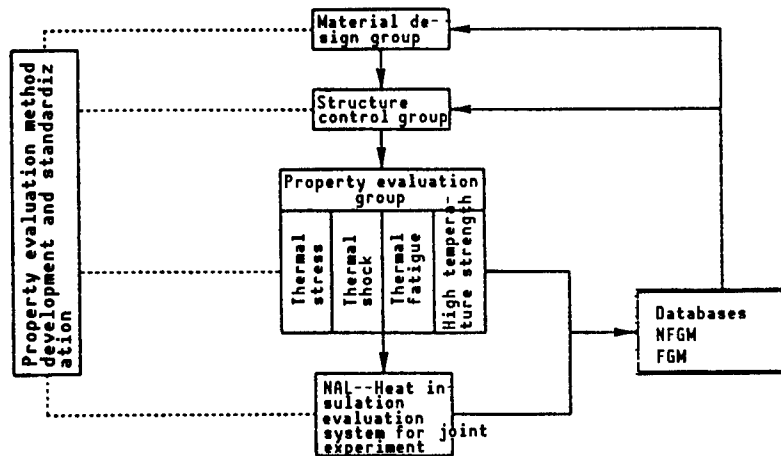


Figure 7. Data Flow for Database Formation for Functionally Gradient Material Development Project

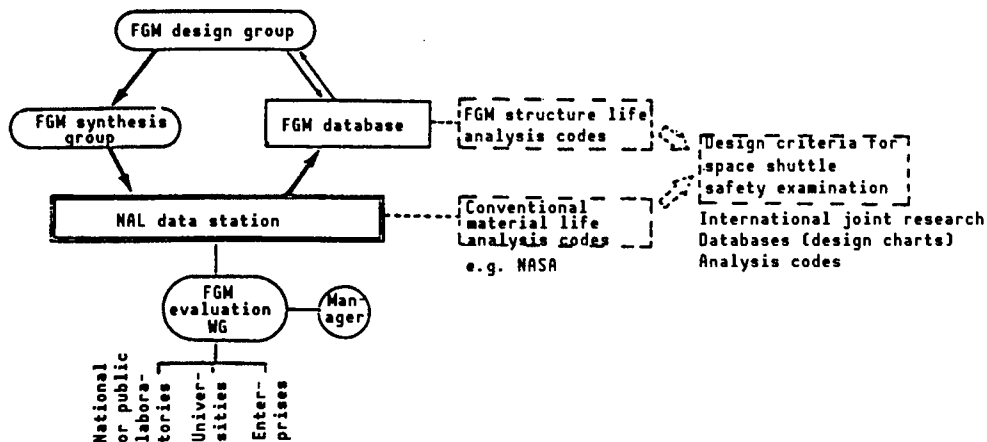


Figure 8. Functionally Gradient Material Database Contents and Utilization

standardizing material evaluation methods for the present functionally gradient material development project.

5. Conclusion

History shows that the success of the U.S. Apollo project was in large part attributable to the adoption of the fracture mechanics concept as well as

the standardization and adoption of a fracture toughness (K_{IC}) test method in connection with the designing of the airframe and fuel tank. To obtain results useful for a subsequent space shuttle development project from the present project for the development of functionally gradient materials effective in thermal stress relaxation, we should learn from the U.S. experience--that is, detailed study to work out a new design concept and material evaluation criteria required to promote the space shuttle development project in the future should be started immediately.

References

1. Japan Atomic Energy Research Institute, "Small Punch Test Method Plan," JAERI-memo 62-193, 1987.
2. National Aerospace Laboratory, "Research on Fracture Strength Evaluation Method for the Development of Functionally Gradient Material Effective in Thermal Stress Relaxation," 1988, being prepared for publication.

- END -